## TITLE

# Single-cell intracellular pH dynamics regulate the cell cycle by timing G1 exit and the G2 transition

## AUTHORS AND AFFILIATIONS

Julia S. Spear[1,2] and Katharine A. White[1,2]

[1]Department of Chemistry and Biochemistry, University of Notre Dame, Notre Dame, IN, USA

[2]Harper Cancer Research Institute, University of Notre Dame, Notre Dame, IN, USA

*To whom correspondence should be addressed: kwhite6@nd.edu

## SUMMARY

Spear et al. characterize an approach for measuring single-cell intracellular pH (pHi) and monitoring single-cell pHi dynamics during cell cycle progression. By tracking pHi in single cells, Spear et al. confirm prior work at the population level showing an increase in pHi at the G2/M transition. However, single-cell pHi measurements reveal new features of pHi dynamics during cell cycle progression, including significantly decreased pHi at the G1/S boundary, S/G2 boundary, and just prior to division, and increases during mid-S phase and G2. Using pHi manipulation, Spear et al. determine that decreased pHi shortens G1 phase and increased pHi elongates G1 phase, indicating low pHi is a cue for G1 exit. S phase progression was also reliant on temporal pHi changes, suggesting pHi dynamics are necessary for cell cycle progression.

## ABSTRACT (160 words)

Transient changes in intracellular pH (pHi) regulate normal cell behaviors like migration and proliferation, while pHi dynamics are dysregulated in cancer. However, it is unclear how spatiotemporal pHi dynamics influence single-cell behaviors. We performed single-cell pHi measurements in normal and cancer cell lines and measured spatiotemporal pHi dynamics during cell cycle progression. Single-cell pHi is dynamic (0.16±0.07 pH units) throughout the cell cycle, with decreased pHi at G1/S, late S, and mitosis and increased pHi in mid-S and G2/M. We next experimentally manipulated pHi and measured effects on cell cycle progression. We show that decreased pHi is a permissive cue for G1 exit, with decreased pHi shortening G1 and increased pHi elongating G1. We also show that dynamic pHi is required for S phase timing, as high pHi elongates S phase and low pHi inhibits S/G2 transition. This work shows dynamic pHi is necessary for cell cycle progression in single cells.

## INTRODUCTION

In normal cells, intracellular pH (pHi) is near neutral (~7.2) while extracellular pH (pHe) is more alkaline (~7.4). Transient changes in pHi driven by ion transporter activity (Boron, 2004) have been shown to regulate normal cell behaviors such as differentiation (Ulmschneider et al., 2016), proliferation (Flinck et al., 2018a), migration (Martin et al., 2011a)(Choi et al., 2013), and apoptosis (Sergeeva et al., 2017). However, most studies of pHi-dependent cell behaviors measure average pHi across a population of cells and perform pHi measurements in non-native cellular environments. Thus, our understanding of the role of spatiotemporal and single-cell pHi dynamics in regulating cell behaviors is limited. Understanding how spatiotemporal pHi dynamics drive single-cell behaviors like division, migration, and apoptosis would enhance mechanistic understanding of pHi dynamics in biology. In addition, a mechanistic understanding of pHi dynamics could lead to new therapeutic routes for limiting pHi-dependent behaviors in diseases with dysregulated pHi, such as cancer (White et al., 2017a; Harguindey et al., 2017) and neurodegeneration (Majdi et al., 2016).

Previous work characterizing single-cell pHi in 2D cell cultures has suggested pHi is heterogeneous (Korenchan and Flavell, 2019). Mouse and human cancer cells were shown to have a distribution of fluorescence ratios when calculated by fluorescence-activated cell sorting (FACS) using the pH-sensitive dye 2',7'-bis(carboxyethyl)-5(6)-Carboxyfluorescein (BCECF) (Lee and Tannock, 1998). This suggests that single-cell pHi is heterogeneous in 2D cell cultures, but the dye was not standardized on the single-cell

level and therefore absolute pHi calculations were not possible. Another limitation of this work is that pHi can be rapidly altered when the cells are trypsinized for FACS analysis, as many ion transporters are also mechanosensitive (Barth and Fronius, 2019; Fuster et al., 2004). In another study using a small number (n<150) of normal and cancerous mouse mammary cells, heterogeneous pHi was linked to metabolic changes (Warburg-like metabolism vs. oxidative phosphorylation) (Lobo et al., 2016). However, the authors did not confirm that single-cell pHi correlated with single-cell metabolic phenotypes. Collectively, these data suggest that single-cell pHi may be heterogeneous in these models and that pHi may report on phenotype or cell state. Unfortunately, the lack of single-cell correlations and the use of non-native environments limit the interpretation of these data.

One pHi-dependent behavior that would benefit significantly from more rigorous single-cell pHi measurements and characterization is proliferation. Cell division is fundamentally a single-cell behavior, but previous studies of cell cycle progression and pHi have been performed at the population level using non-native environments (Taylor and Hodson, 1984; Flinck et al., 2018b; Putney and Barber, 2003) or using lower order organisms (Gillies and Deamer, 1979; Aerts et al., 1985; Karagiannis and Young, 2001).

The first experiments identifying a relationship between cell cycle and pHi used unicellular organisms, such as tetrahymena (Gillies and Deamer, 1979), *Dictyostelium* (Aerts et al., 1985), and *S. pombe* (Karagiannis and Young, 2001). In tetrahymena, two increases in pHi (0.4 pH units) were observed pre- and post-S phase (Gillies and Deamer, 1979).

85 However, all pHi changes were measured at the population level and used harsh
86 synchronization techniques (starvation and heat shock) that disrupt essential cell
87 metabolic functions. In *Dictyostelium*, increased pHi (~0.2 pH units) was measured during
88 S phase and when pHi was artificially increased, DNA replication and protein synthesis
89 were increased as well (Aerts et al., 1985). This indicates that high pHi may drive S phase
90 progression and S phase-related cell functions. However, no timing or delays in S phase
91 progression were noted and only population-level pHi measurements were made. In
92 conflict with the two previous studies, no evidence was found for a relationship between
93 cell cycle and pHi in *S. pombe* using a genetically-encoded pHi biosensor (pHluorin)
94 (Karagiannis and Young, 2001). Thus, the existing data in unicellular organisms is
95 inconsistent in whether pHi regulates (or times) cell cycle progression.
96 While some essential cell functions are evolutionarily conserved, pHi fluctuations in
97 unicellular organisms may not be recapitulated in multicellular models. However, some
98 studies in animal cell models have also shown a relationship between pHi and cell cycle
99 progression. In quiescent populations of human tumor cells, it was shown that a narrow
100 range of pHe values (pH 6.8 to 7.2) can recruit cells into the cell cycle (Taylor and Hodson,
101 1984). This suggests that a defined range of pHe is required for normal proliferation, but
102 they did not measure pHi which can be altered in response to pHe changes (Deutsch et
103 al., 1982). In population-level analyses of pHi in thymidine-synchronized MCF-7 breast
104 cancer cells, pHi was found to fluctuate after thymidine release but no statistical
105 significance was noted (Flinck et al., 2018b). Strengthening the link between pHi and cell
106 cycle regulation, knockdown of the $Na^+/H^+$ exchanger (NHE1) and $Na^+$-$HCO_3^-$ transporter
107 (NBCn1) caused elongation of S phase and a delay in the G2/M transition (Flinck et al.,

108 2018b), but no single-cell pHi measurements were made. In another example, an
109 increase in pHi driven by NHE1 was found to time the G2/M transition (Putney and Barber,
110 2003). However, the experiments in these studies were carried out using population-level
111 assays and performed using environmental (pHe) changes or genetic ion transporter
112 knockdown. As ion transporters also serve scaffolding and signaling roles, knockdown
113 can produce transport-independent effects on cell biology. Although these studies lay a
114 framework for a relationship between pHi and cell cycle, there is a need for single-cell pHi
115 measurements in native environments to elucidate how temporal pHi dynamics regulate
116 cell cycle progression.
117
118 Here, we present single-cell pHi measurements under physiological conditions in both
119 asynchronous and synchronized cell populations to determine if pHi regulates cell cycle
120 progression at the single-cell level. First, we show that asynchronous lung cancer cells
121 have increased pHi compared to lung epithelial cells and the pHi distributions were similar
122 between all cell populations. To investigate pHi during specific cell cycle phases, we
123 synchronized cells in G1 (Palbociclib) and early S phase (thymidine) and measured pHi
124 as cells were released using endpoint and time-lapse microscopy. We determined that
125 single-cell pHi oscillated during cell cycle progression: pHi significantly decreased at
126 G1/S, S/G2, and mitosis, and increased during mid-S and G2/M. Using pHi manipulation
127 and Fluorescent Ubiquitination-based Cell Cycle Indicator (FUCCI) reporters, we
128 determined dynamic pHi is necessary for normal progression through the cell cycle. We
129 show that low pHi is a cue for G1 exit and normal S phase duration requires both a pHi
130 increase and decrease. This work highlights the advantages of using single-cell pHi

131 measurements to investigate single-cell behaviors like cell cycle, as we show previously
132 uncharacterized pHi dynamics regulating G1 exit and S phase.
133
134 **RESULTS**
135 **Single-cell pHi in asynchronous cell populations is heterogenous, but is increased**
136 **in transformed and metastatic lung cells compared to normal cells**
137 In normal epithelial cells, pHi is near neutral (~7.2), while cancer cells have a constitutively
138 increased pHi (pHi>7.4). This constitutively increased pHi occurs early in cancer
139 development (Reshkin et al., 2000; Cardone et al., 2005) and promotes pHi-dependent
140 behaviors such as proliferation, cell invasion, and metastasis (White et al., 2017a). Our
141 first goal was to determine if we could accurately quantify single-cell pHi distributions
142 within various clonal lung cell lines (normal and cancerous). We used a genetically-
143 encoded biosensor, mCherry-pHluorin (mCh-pHl), for our applications (Koivusalo et al.,
144 2010). The mCh-pHl biosensor has been used to measure pHi in cultured cells (Koivusalo
145 et al., 2010; Choi et al., 2013) and tissues (Grillo-Hill et al., 2015) and has a dynamic
146 linear range between pH 6.5 and 8.0 (Grillo-Hill et al., 2014). Briefly, direct measurement
147 of pHi in single living cells can be achieved by performing ratiometric imaging of
148 pHluorin/mCherry fluorescence intensities. Fluorescence of pHluorin is pH-sensitive in
149 the physiological range while mCherry fluorescence is not and can be used to normalize
150 biosensor expression. At the end of the experiments, single-cell standardization is
151 performed using buffers of known pH containing the protonophore nigericin (Fig. 1A, see
152 methods for details). This method of pHi measurement avoids issues of uneven dye

153 loading, washout, and photobleaching that are associated with pH-sensitive dyes (Grillo-
154 Hill et al., 2014).
155
156 We first examined whether asynchronous single-cell pHi measurements under
157 physiological conditions could recapitulate population-level averages while also reflecting
158 physiological heterogeneity. We stably expressed mCh-pHl in normal lung epithelial cells
159 (NL20), primary tumor site-derived lung cancer cells (A549), and metastatic site-derived
160 lung cancer cells (H1299). We confirmed that population pHi measurements in the clonal
161 biosensor lines (NL20-mCh-pHl, A549-mCh-pHl and H1299-mCh-pHl) were unchanged
162 compared to matched parental cell lines using a standard plate reader assay with the pH-
163 sensitive dye BCECF (Grillo-Hill et al., 2014) (Fig. S1). We next measured single-cell pHi
164 in individual NL20-mCh-pHl (Fig. 1B), A549-mCh-pHl (Fig. 1C), and H1299-mCh-pHl (Fig.
165 1D) cells. Representative pHluorin and mCherry channels and single-cell standardization
166 lines can be found in Fig. S2. To quantify heterogeneity in these clonal cell lines, we
167 prepared distribution histograms of single-cell pHi measurements. We found that the pHi
168 of primary tumor cells (A549-mCh-pHl) (Fig. 1F; 7.54±0.07) was increased compared to
169 normal lung epithelial cells (NL20-mCh-pHl) (Fig. 1E; 7.42±0.07). Importantly, metastatic
170 tumor cells (H1299-mCh-pHl) had the highest median pHi (Fig. 1G; 7.65±0.07), which
171 was significantly higher than both the normal and primary tumor clonal cell lines. These
172 data show the advantages of measuring single-cell pHi under physiological culture
173 conditions that match population averages, but also provide pHi distributions lost at the
174 population level. These data also show that pHi is heterogeneous even in clonal,

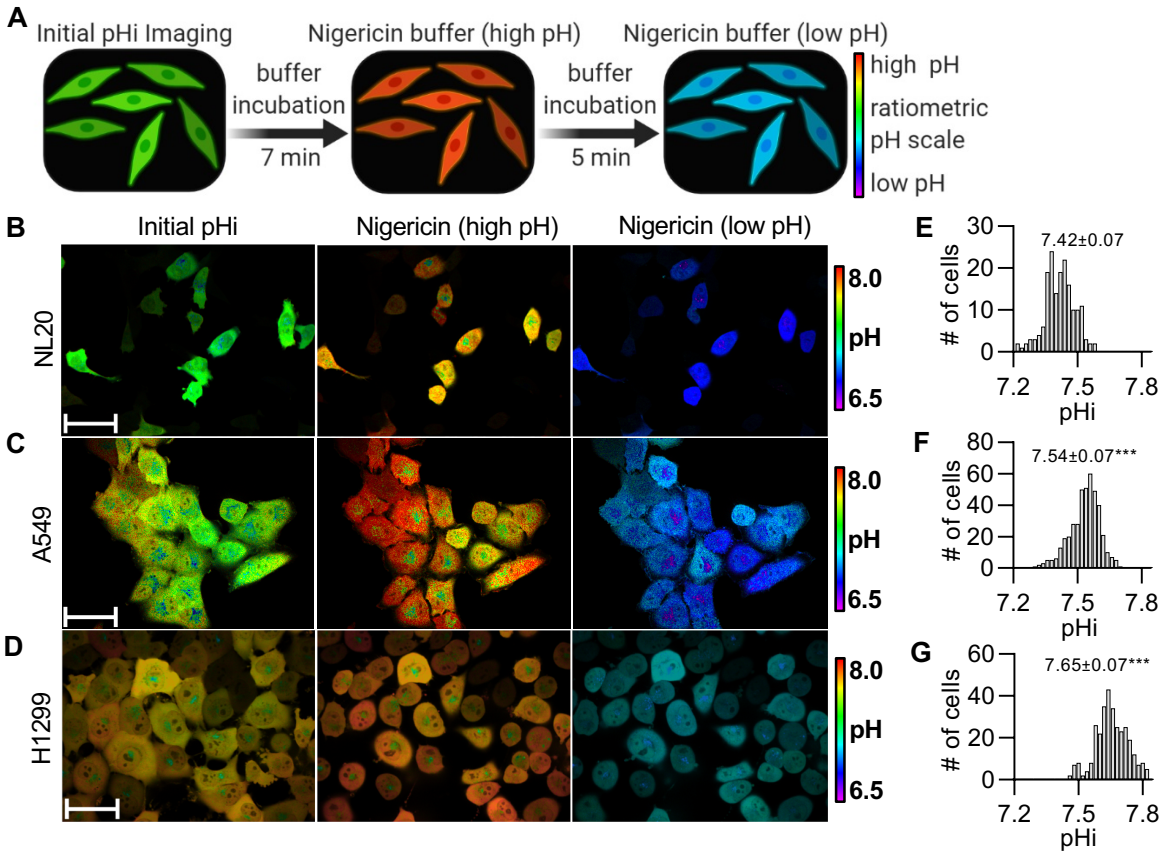


genetically identical, cell lines, suggesting pHi may be a biomarker for non-genetic cell phenotype.

**Figure 1: Intracellular pH is heterogeneous in normal and cancerous lung cell lines and median pHi significantly increases in cancer cells.**
A) Schematic of single-cell pHi measurements using a stably expressed pH biosensor, mCherry-pHluorin (mCh-pHl), and the protonophore nigericin to standardize the biosensor (see methods for details). B-D) Representative images of pHi measurements and standardization in B) NL20, C) A549, and D) H1299 cells stably expressing mCh-pHl. Ratiometric display of pHluorin/mCherry fluorescence ratios, scale bars: 50 µm. E-G) Histograms of single-cell pHi in E) NL20 (n=173, 3 biological replicates), F) A549 (n=424, 4 biological replicates), and G) H1299 (n=315, 3 biological replicates). Histograms are binned at 0.02 pH units. Above histograms, median±S.D. Significance was determined by a Mann Whitney test. (***p<0.001, compared to NL20).

191 From our data, we measured a range of pHi values within single distributions of clonal
192 cell lines, suggesting pHi heterogeneity may reflect non-genetic, phenotypic
193 heterogeneity. We noted that the single-cell pHi measurements were performed in
194 asynchronous cell populations (Fig. 1) and prior work suggests pHi is dynamic during the
195 mammalian cell cycle (Putney and Barber, 2003; Flinck et al., 2018b). However, those
196 experiments were performed at the population level and used non-physiological
197 environments (FACS) that can produce artifactual effects on pHi. With our ability to
198 measure single-cell pHi in physiological environments, we sought to measure pHi
199 dynamics during cell cycle phases and characterize the regulatory effect of pHi on cell
200 cycle progression in single cells.
201
202 **Cells released from G1 synchronization have dynamic pHi**
203 Using mCh-pHl and cell synchronization methods, we measured single-cell pHi dynamics
204 during cell cycle progression. We synchronized H1299-mCh-pHl cells using Palbociclib,
205 which blocks the phosphorylation of the retinoblastoma protein and synchronizes cells
206 prior to the G1 checkpoint (Liu et al., 2018) (Fig. 2A). It has recently been shown that
207 Palbociclib is an efficient G1 synchronizer in H1299 cells, with nearly 85%
208 synchronization after 24 h treatment and minimal DNA damage (Trotter and Hagan,
209 2020). After synchronization (0.1 μM Palbociclib), cells were imaged at 0, 4, 8, 12, 24,
210 and 36 hours (h) after release (Fig. 2B) and single-cell pHi distributions were measured
211 (Fig. 2C). Qualitatively, we noticed cells were larger at earlier time points (0-4 h) and
212 starting at 12 h cells exhibited altered morphology that could indicate mitosis (Fig. 2B).
213 Through ratiometric imaging, we found cells had low pHi from 4-8 h and high pHi at 24 h

214 (Fig. 2B). In this representative replicate, we observed single-cell pHi significantly
215 decreased between 0 and 4 h, significantly increased between 4 and 8 h, decreased
216 between 8 and 12 h, and increased again between 12 and 24 h (Fig. 2D). This data
217 suggests that pHi is dynamic during cell cycle progression with multiple fluctuations in pHi
218 after synchronization release.

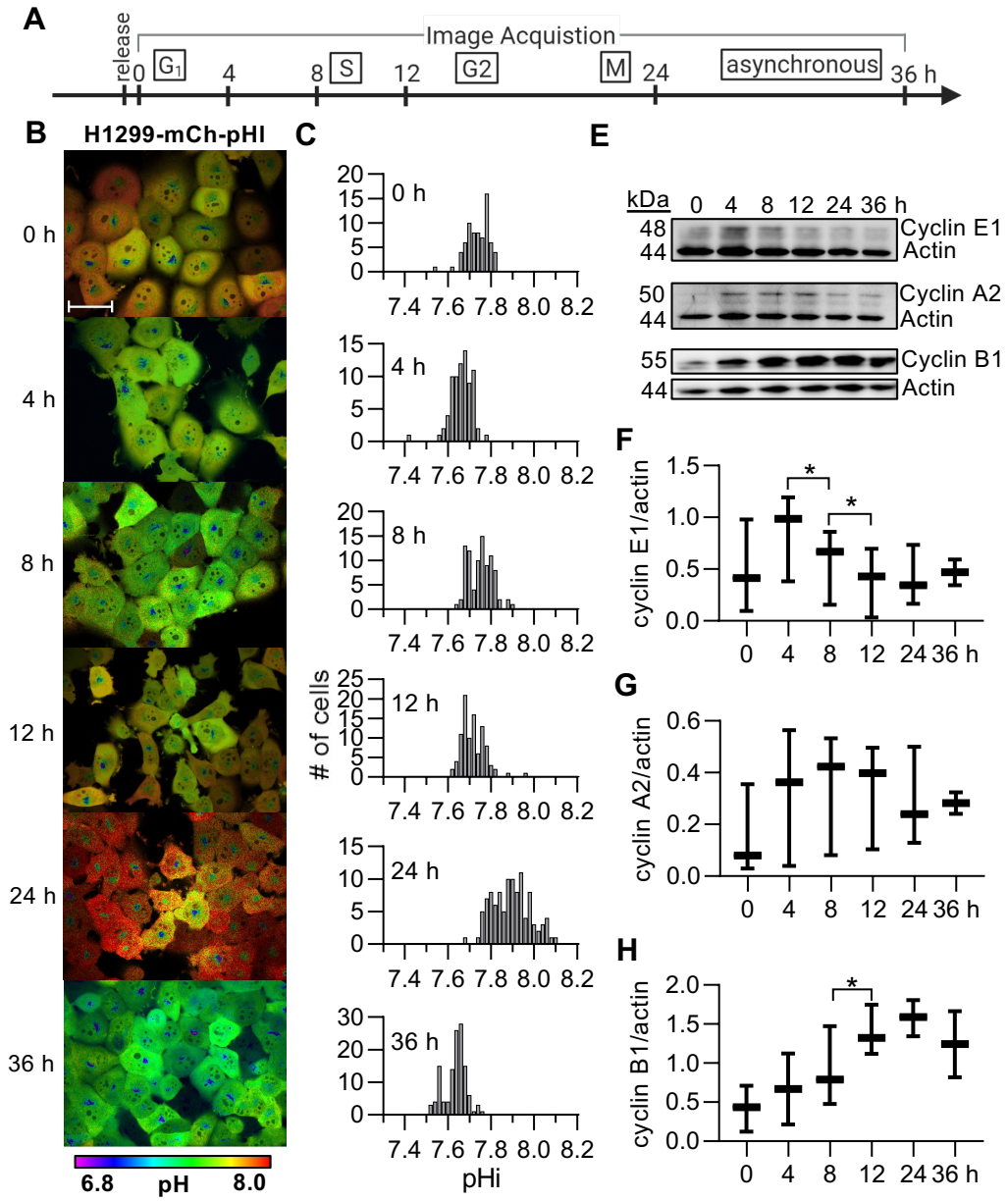


D

| | H1299-mCh-pHI |
|---|---|
| 0 h | 7.75±0.05 |
| 4 h | 7.67±0.04*** |
| 8 h | 7.75±0.05*** |
| 12 h | 7.71±0.05* |
| 24 h | 7.90±0.09*** |
| 36 h | 7.65±0.05*** |

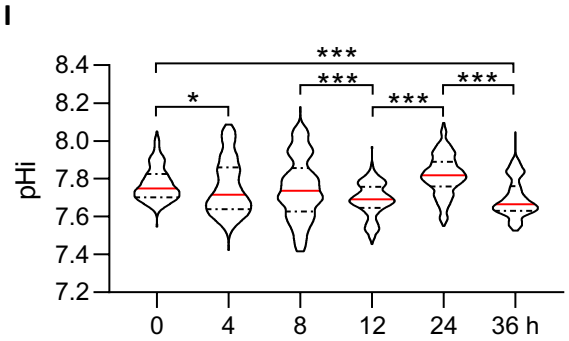


**Figure 2: Intracellular pH is dynamic following G1 synchronization and correlates with cyclin levels.** A) Schematic of image acquisition after Palbociclib synchronization.

221 B) Representative images of H1299-mCh-pHl cells at indicated time points after release.
222 Ratiometric display of pHluorin/mCherry fluorescence ratios. Scale bar: 50 μm. C)
223 Histograms of single-cell pHi data collected as in B, from one biological replicate.
224 Histograms binned at 0.02 pH units. Additional replicates shown in Fig. S3. D) Medians
225 and standard deviations at each time point shown in C. E) Representative immunoblots
226 for cyclin E1, A2, and B1 with respective actin loading controls. Box and whisker plots of
227 F) cyclin E1, G) cyclin A2, and H) cyclin B1 immunoblot data across 3 biological replicates.
228 Additional replicates shown in Fig. S3. I) Violin plots of raw pHi across 3 biological
229 replicates. In D and I, significance was determined according to a Kruskal Wallis test with
230 Dunn's multiple comparisons correction. In F-H, significance was determined by a paired
231 t-test. In D and F-I, each time point was compared to the preceding time point and in I, 0
232 h was compared to 24 h. (*$p<0.05$; ***$p<0.001$).
233

234 We confirmed that Palbociclib appropriately synchronized the cells by immunoblotting for
235 cyclins from matched cell lysates (Fig. 2E). Cyclin E1 regulates G1/S (Siu et al., 2012),
236 cyclin A2 regulates S and G2 phases (De Boer et al., 2008), while cyclin B1 regulates G2
237 and is degraded by the start of anaphase in mitosis (Chang et al., 2003). We observe that
238 cyclin E1, a marker of G1/S, significantly increases from 0 to 4 h, which is expected for a
239 cell population properly synchronized in G1 phase (Fig. 2F). These cells undergo mitosis
240 approximately 24 h post-Palbociclib release because cyclin B1 levels, an inducer of G2/M,
241 increased from 8 to 12 h and peaked 24 h post-release (Fig. 2H). By 36 h, protein
242 abundance was similar across all cyclins, as expected in an asynchronous population.
243 Cyclin immunoblots and pHi agreed across 3 biological replicates, and additional blots
244 are shown in Fig. S3. This suggests that our experimental assay using Palbociclib to
245 synchronize cells at G1 is capturing progression through a complete cell cycle.

246
247 When pHi measurements on Palbociclib-treated cells were compared over three
248 biological replicates, we found that pHi significantly decreased at the G1/S transition (4
249 h, 7.75±0.15) and in late S phase (12 h, 7.69±0.09), significantly increased at G2/M (24
250 h, 7.82±0.11) (Fig. 2I), and then significantly decreased once more at the end of the

251 experiment in asynchronous cells (36 h, 7.67±0.10) (Fig. 2I). These pooled data
252 recapitulate the wave-like pHi pattern observed in the individual replicate. Individual pHi
253 distribution plots for the additional replicates are shown in Fig. S3. To assess if Palbociclib
254 alters resting pHi on its own, we pooled the synchronized time points (Fig. 2I, 0-24 h) and
255 compared these data to pHi measurements from the endpoint Palbociclib data (Fig. 2I,
256 36 h) and to untreated, asynchronous H1299-mCh-pHI pHi data (Fig. 1G). Palbociclib-
257 treated cells had a significantly higher pHi than the untreated, asynchronous cells,
258 indicating that Palbociclib synchronization may also alter pHi homeostasis (Fig. S3C).
259 However, this increase in resting pHi is uniform and we are still able to measure significant
260 fluctuations in pHi, with decreasing pHi at G1/S and late S, and increasing pHi leading to
261 G2/M.
262

263 **Cells exhibit cell cycle-linked pHi dynamics independent of cell cycle**
264 **synchronization method**

265 Because Palbociclib synchronization altered resting pHi (Fig. S3C), we wanted to confirm
266 that the pHi dynamics observed in these experiments were linked to cell cycle phase and
267 not an artifact of the Palbociclib synchronization method. We synchronized H1299-mCh-
268 pHI cells using a double-thymidine block (Chen and Deng, 2018) which halts cells in early
269 S phase. Thymidine acts as a DNA synthesis inhibitor by accumulating dTTP and
270 depleting dCTP within the cell (Bjursell and Reichard, 1973; Bolderson et al., 2004). We
271 synchronized H1299-mCh-pHI cells and imaged them at 0, 4, 8, 12, and 24 h after
272 thymidine release (Fig. 3A-B). Qualitatively, we noticed cells were larger at 0 h and
273 starting at 8 h had distinct cell rounding and smaller apparent cell size that may indicate

274 mitotic cells (Fig. 3B). In this representative replicate, we observed single-cell pHi
275 significantly decreased between 0 and 4 h, significantly increased between 4 and 8 h,
276 decreased between 8 and 12 h, and increased again between 12 and 24 h (Fig. 3C-D).
277 This general observation supports our data from cells released earlier in the cell cycle
278 (Palbociclib, G1) (Fig. 2) and suggests that pHi is dynamic during the cell cycle regardless
279 of the synchronization method used.
280
281 We again confirmed that the treatment appropriately synchronized the cells by
282 immunoblotting for cyclins from matched cell lysates (Fig. 3E). We found that cyclin E1,
283 a marker of G1 and early S phase, is highest at 0 h, as expected for a cell population
284 properly synchronized in early S phase (Fig. 3F). These cells undergo mitosis
285 approximately 8 h after thymidine release because cyclin A2, which is degraded before
286 the G2/M checkpoint, was highest at 4 h and significantly decreased by 8 h, showing
287 transition to late G2 (Fig. 3G). Confirming this, we observed that cyclin B1 levels, an
288 inducer of G2/M, increased from 0 to 4 h and peaked 8 h after release (Fig. 3H). Cyclin
289 E1 levels increased again by 12 h, suggesting most cells in this assay completed the cell
290 cycle and progressed back to G1 phase (Fig. 3F). By 24 h, protein abundance was similar
291 across all cyclins, as we would expect in an asynchronous population. Immunoblots for
292 additional replicates are shown in Fig. S4. These cyclin results match previously
293 published data on synchronized H1299 cell populations (Chen and Deng, 2018),
294 supporting that the thymidine protocol appropriately synchronized the cells.
295

296 When pHi was compared over four biological replicates, we found that the median pHi of
297 the cell populations decreased significantly at 4 h (late S phase), increased from 4 to 8 h
298 (G2/M), and decreased once more from 8 to 12 h (M/G1) (Fig. 3I). This preserves the
299 wave-like pHi pattern measured in the individual replicate. Individual pHi distribution plots
300 for additional replicates are shown in Fig. S4. In the merged replicate data, there was no
301 significant difference in pHi between 12 h and 24 h, but at 24 h, pHi was significantly lower
302 than at 0 h (Fig. 3I). Confirming thymidine treatment did not alter pHi, we did not observe
303 any significant differences in pHi when comparing pooled synchronized data (Fig. 3I, 0-
304 12 h) to pHi measurements from both asynchronous thymidine data (Fig. 3I, 24 h) and
305 untreated, asynchronous H1299-mCh-pHI cells (Fig. 1G) (Fig. S4C). Our thymidine pHi
306 data recapitulate both the decreased pHi in late S phase and increased pHi during G2/M
307 that we measured after release from Palbociclib, while also revealing a pHi increase
308 during early S phase.

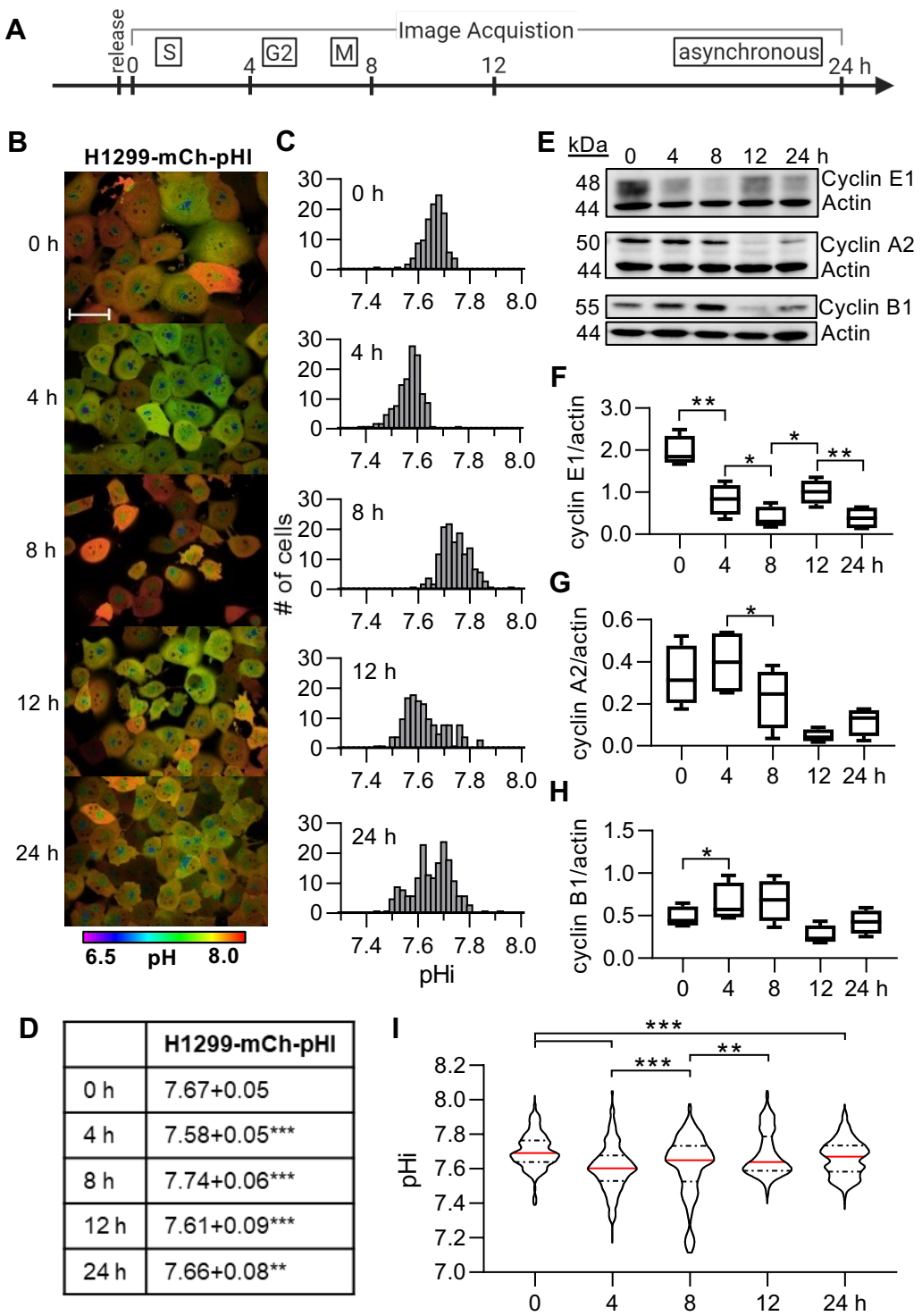


| | H1299-mCh-pHI |
|---|---|
| 0 h | 7.67+0.05 |
| 4 h | 7.58+0.05*** |
| 8 h | 7.74+0.06*** |
| 12 h | 7.61+0.09*** |
| 24 h | 7.66+0.08** |

**Figure 3: Intracellular pH is dynamic after release from early S phase in H1299-mCh-pHI cells and correlates with cyclin levels.**
A) Schematic of image acquisition after a double-thymidine synchronization. B) Representative images of H1299-mCh-pHI cells at indicated time points after release. Ratiometric display of pHluorin/mCherry fluorescence ratios, scale bar: 50 µm. C) Histograms of single-cell pHi data collected in B, from one biological replicate. Histograms

binned at 0.02 pH units. Additional replicates are shown in Fig. S4. D) Table of pHi values from data in C (median±S.D.). E) Representative immunoblots for cyclin E1, A2, and B1 with respective actin loading controls. Box and whisker plots of F) cyclin E1, G) cyclin A2, and H) cyclin B1 immunoblot data across 4 biological replicates. Additional replicates shown in Fig. S4. I) Violin plots of raw pHi across 4 biological replicates. In D and I, significance was determined using a Kruskal Wallis test with Dunn's multiple comparisons correction. In F-H, significance was determined by a paired t-test. In D and F-I, each time point was compared to its preceding time point and in I, 0 h compared to 24 h. (*$p<0.05$; **$p<0.01$; ***$p<0.001$).

To confirm results in H1299-mCh-pHl cells, we similarly synchronized A549-mCh-pHl with a double-thymidine block and observed similar pHi dynamics to H1299-mCh-pHl cells (Fig. S5). Cells were morphologically similar in size to H1299-mCh-pHl populations (Fig. S5A) at respective time points, indicating cell growth leading to mitosis (Fig. S5A; 0-4 h) and mitotic cell rounding during M phase (Fig. S5A; 8 h). The measured pHi values oscillated similarly to H1299-mCh-pHl cells with a decrease from 0 h to 4 h, an increase from 4 h to 8 h, and decreases at 12 h and 24 h (Fig. S5B-C). Again, synchronization by double-thymidine block was confirmed in A549-mCh-pHl cells using cyclin immunoblots, where cyclin A2 (S/G2) peaked at 4 h, cyclin B1 (G2/M) peaked at 8 h, and both proteins were low at 12 h indicating the start of a new cycle with cells in G1 (Fig. S5D). Single-cell pHi distribution plots and western blots for additional replicates are shown in Fig. S6. Like H1299-mCh-pHl cells, collective pHi in A549-mCh-pHl cells across 4 biological replicates significantly increased from 4 h to 8 h (G2/M) and decreased following mitosis at 12 h (Fig. S5E). Observing the same cell-cycle-linked pHi dynamics across different cell models suggests the increases leading to division (G2/M, 4-8 h) and decreases after division (G1, 8-12 h) may be necessary for division timing and re-entry into the cell cycle.

342 From these varying methods of cell synchronization and combination of pHi endpoint
343 assays through cyclin immunoblots, we conclude that pHi is dynamic through the cell
344 cycle at the single-cell level: pHi decreases during G1/S, increases in early S phase,
345 decreases leading to S/G2, increases prior to G2/M, and drops in pHi following mitosis.
346 While the pHi values are quantified from single-cell measurements, these are endpoint
347 assays with population-level comparisons. We next asked whether pHi dynamics within
348 single, dividing H1299-mCh-pHl cells followed a similar oscillating pHi pattern when
349 tracked over time.
350

351 **Single cells alkalize prior to G2/M, followed by rapid acidification during mitosis**
352 **and pHi recovery in daughter cells**

353 In the previous experiments, cells from matched populations were identically treated and
354 released from synchronization for sampling at time points after release. Although these
355 time points showed that single-cell pHi distributions fluctuate with cell cycle progression,
356 the snapshots may not reflect continuous single-cell pHi dynamics or single-cell, cell cycle
357 progression phenotypes. To address this limitation, we established a time-lapse approach
358 to track pHi dynamics over an entire cell cycle in a single cell.
359

360 We synchronized H1299-mCh-pHl cells with a double thymidine block as in Fig. 3 and
361 imaged cells every 20 minutes for 24 h following thymidine release to acquire dynamic
362 single-cell pHi measurements. We observed bursts of mitotic cells at 15 h±4 h, indicating
363 thymidine was synchronizing individual cells. Representative stills of ratiometric time-
364 lapse pHi imaging in a dividing cell are shown (Fig. 4A, Video S1). For this cell, pHi

365 quantification shows increasing pHi through late S and G2 phases (as determined by Fig.
366 3 cyclin data), acidification just before mitosis, and pHi recovery in daughter cells (Fig.
367 4B). To investigate and compare trends in single-cell pHi dynamics over the cell cycle,
368 we selected prophase as a "normalization point" for each individual dividing cell.
369 Prophase was chosen because DNA condensation was easily identified using live-cell
370 DNA staining. When pHi dynamics were plotted for 39 dividing cells, we observed a
371 significant period of alkalization that began ~11 h prior to division and persisted until
372 prophase (Fig. 4C). Parent cells that divided within the 24 h period showed a significantly
373 higher median pHi increase (0.16±0.07; Fig. 4D) when compared to nondividing cells
374 (0.10±0.03; Fig. 4D). These data suggest that increased pHi dynamics may be required
375 to signal a cell to divide. Prior work on pHi in migration (Martin et al., 2011b) and cell cycle
376 progression (Flinck et al., 2018a) show pHi increases of 0.2 at the population level are
377 capable of altering these cell behaviors at the population level. These single-cell data
378 suggest that the pHi dynamics measured in dividing single cells are within the reported
379 physiological range for pHi-dependent regulation of cell behaviors.
380
381 The single-cell pHi increases measured prior to division in the time-lapse experiments
382 correlate with the increased pHi observed during G2/M in the discontinuous endpoint data
383 (Fig. 2I, 3I, S5E). Interestingly, these single-cell data also reveal a significant acidification
384 event in single cells following prophase, which may correlate with the acidification
385 observed in the discontinuous H1299-mCh-pHl and A549-mCh-pHl cells after mitosis
386 (Fig. 3I, S5E). Although we were able to measure pHi dynamics during G2/M via DNA
387 condensation, we were not able to confidently measure where the S/G2 transition

388 occurred. Therefore, we could not correlate these data with additional pHi changes
389 observed in the endpoint data, including decreased pHi during S phase (Fig. 2I, 8-12h;
390 Fig. 3I, 4 h).
391

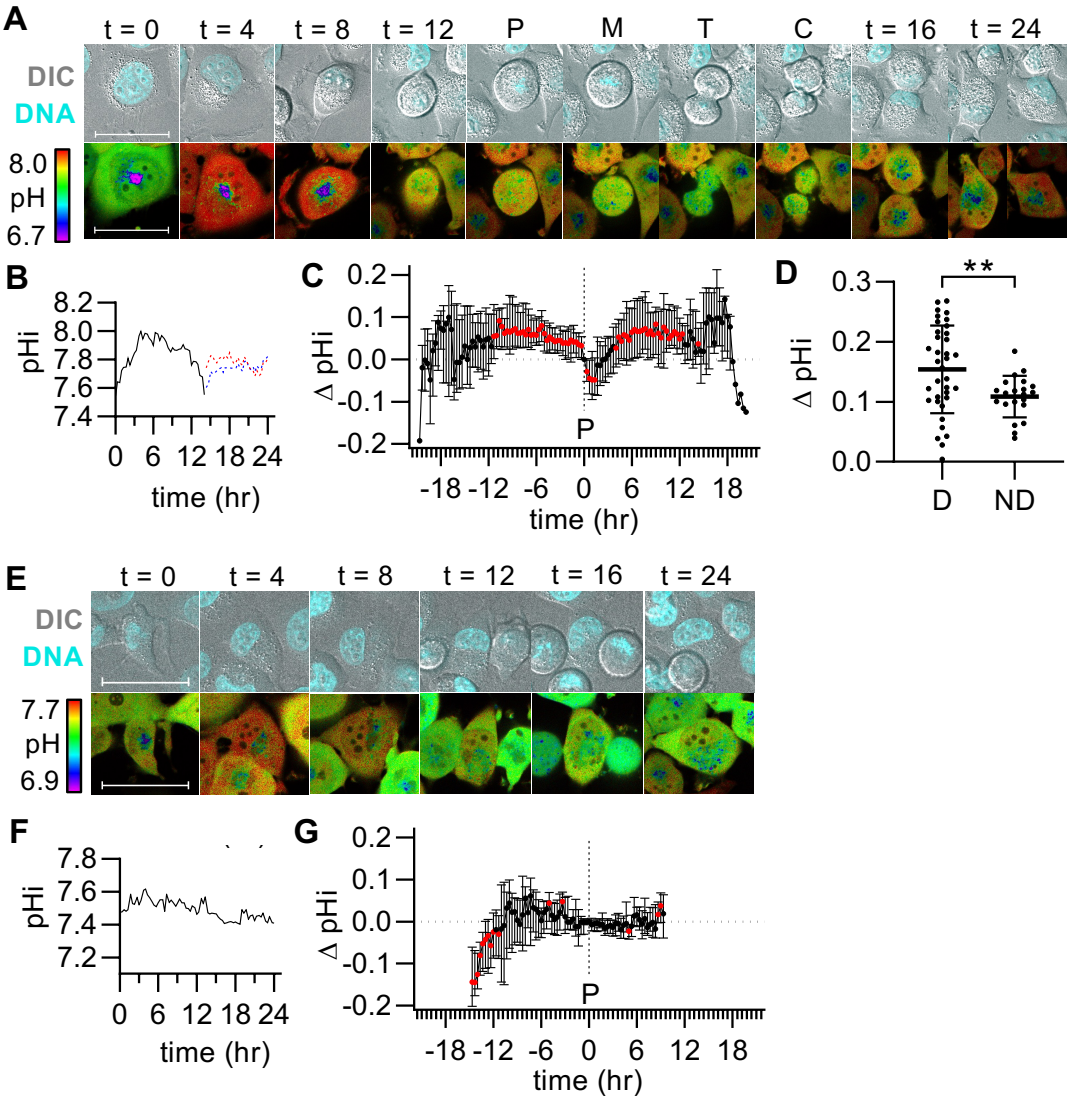


392 **Figure 4: Intracellular pH increases leading to G2/M, followed by rapid acidification**
393 **prior to division and recovery of daughter cells.**
394 A) Representative stills of Video S1 of a dividing H1299-mCh-pHl cell at indicated time
395 (h). Top is Hoescht dye (DNA, cyan) and DIC merge. Bottom is ratiometric display of
396 pHluorin/mCherry fluorescence ratios, scale bars: 50 µm. B) Traces of calculated pHi
397 values of the cell in A) (black, solid line) and in daughter cells (red and blue dotted lines).

C) pHi changes in dividing cells, relative to pHi at prophase (P) for each individual cell (median±IQ range, n=39, 3 biological replicates). Significance determined by a one-sample Wilcoxon test compared to 0 (red points, *p<0.05). D) Scatter plot of max pHi change in individual dividing (D) and non-dividing (ND) cells (mean±SD). Significance determined by an unpaired t-test (**p<0.01). E) Representative stills of Video S2 of a non-dividing H1299-mCh-pHl cell at indicated time (h). Top is Hoescht dye (DNA, cyan) and DIC merge. Bottom is ratiometric display of pHluorin/mCherry fluorescence ratios, scale bars: 50 μm. F) Trace of pHi values of cell in E) (black, solid line) over time. G) pHi changes in non-dividing cells, relative to the pHi at average time of prophase (determined from dividing cell data) (median±IQ range, n=22, from 3 biological replicates). Significance determined by a one-sample Wilcoxon test compared to 0 (red points, *p<0.05).

Although we saw a burst of mitotic cells after thymidine release that validates our synchronization was effective, there was some variability in the timing of prophase (Fig. S7A) and heterogeneity in the magnitude of pHi changes from prophase (Fig. 4D, S7B). To confirm that alkalinization was correlated with cell-cycle timing vs. imaging timing, we binned dividing cells according to prophase time. We observed significant alkalizations in each group pre- and post-prophase, with a significant alkalinization point at ~5 h prior to prophase regardless of timing of prophase (Fig. S7C). Previous data using FUCCI cell cycle reporters found late S/G2 length ranging from ~5-13 h in H1299 cells (Rajal et al., 2021). Additionally in our own data (shown below), we measured 4.3 h as the average G2 length. Taken together, these data suggest that the increase in pHi at 5 h may be occurring at the S/G2 transition. This significant pHi increase is also observed in the time-lapse traces (Fig. 4C) and the single-cell endpoint data corresponding to S/G2 cyclin markers (Fig. 2I, 12 h; Fig. 3I, 4 h). These data suggest that increased pHi may be a permissive cue for G2 phase entry.

The single-cell time-lapse analysis allows us to differentiate between cells that undergo mitosis and cells that do not. If pHi dynamics are a sufficient regulator of cell cycle progression, we may expect to see attenuated pHi dynamics in non-dividing cells. To test

428 this hypothesis, we quantified pHi from non-dividing cells in our dataset. Representative
429 stills of ratiometric time-lapse pHi imaging in a non-dividing cell are shown in Fig. 4E
430 (Video S2). This non-dividing cell showed attenuated pHi dynamics compared to dividing
431 cells (Fig. 4F). To compare trends in single-cell pHi dynamics for non-dividing cells, delta
432 pHi was calculated for each non-dividing cell from the average prophase timing in dividing
433 cells (15 h) (Fig. 4G). When pHi data from the 22 non-dividing cells were analyzed, we
434 observed attenuated pHi dynamics with the only significant changes coming from a short
435 period of alkalization after release (Fig. 4G). Importantly, the significant alkalization we
436 observe in dividing cells in the ~5 hours prior to prophase (Fig. 4C, Fig. S7C) is not
437 observed in the non-dividers, indicating that single-cell pHi dynamics may be correlated
438 with (or regulate) single-cell cell cycle progression.
439
440 S phase is associated with increased protein expression (Aviner et al., 2015). To confirm
441 that the alkalinization we observed in S phase is not an artifact of increased mCh-pHl
442 biosensor expression, we tracked mCherry and pHluorin intensities over time in both
443 dividers and non-dividers (Fig. S8). If the alkalinization is artifactual, we would expect to
444 see increases in the pH-insensitive mCherry fluorescence in dividers specifically,
445 indicating increased protein expression during S phase. Instead, we observe that
446 mCherry fluorescence similarly decreases after initial acquisition (photobleaching)
447 followed by a stabilization in both dividers and non-dividers (Fig. S8A). Furthermore, the
448 pHluorin increases observed over time in dividing cells are not correlated with increased
449 mCherry fluorescence, which indicates pHluorin increases are not due to increases in
450 biosensor expression (Fig. S8B-C).

451

452 **Dysregulated pHi dynamics affect cell cycle phase duration and cause phase-**
453 **specific arrests**

454 We have shown that after synchronization with Palbociclib (Fig. 2) and thymidine (Fig. 3),
455 pHi is dynamic and correlates with cell cycle phases. To compare pHi data from both
456 synchronization techniques, we aligned pHi data (Fig. 2I, Fig 3I) according to significantly
457 increased cyclin B1 expression (Fig. 2H, Fig. 3H) and found oscillating pHi dynamics
458 through the cell cycle (Fig. 5A). We observed that pHi decreases during G1/S, increases
459 in mid-S phase, decreases leading to S/G2, and increases leading to G2/M (Fig. 5A). In
460 addition, our time-lapse data uncovered rapid acidification during M phase leading to
461 division (Fig. 4C). These data suggest a correlation between pHi and cell cycle
462 progression, but to determine a causal relationship, we needed the ability to change pHi
463 and determine effects on cell cycle phases in real-time. To do this, we used established
464 pHi manipulation techniques (White et al., 2017b; Larsen et al., 2012) and the FUCCI cell
465 cycle reporter to track single cells during cell cycle progression using time-lapse
466 microscopy.

467

468 FUCCI reporters use regulatory domains of cell-cycle proteins to differentially express
469 fluorescent proteins and report on cell cycle progression in single cells (Fig. 5B). We
470 selected the PIP-FUCCI reporter, which allows improved delineation of S phase (Grant
471 et al., 2018) compared to older FUCCI variants. The PIP-FUCCI reporter fluorescence is
472 driven by regulatory domains PCNA interacting protein degron from human $Cdt1_{1-17}$ (PIP)
473 fused to mVenus and $Geminin_{1-110}$ fused to mCherry. PIP-mVenus accumulates in the

474 nucleus during G1 and is rapidly lost the during onset of DNA replication (S phase). At
475 the beginning of S phase, mCherry-Geminin accumulates and is expressed throughout
476 S, G2, and M phases. During the S-G2 transition, mVenus accumulates again, and both
477 mVenus and mCherry are co-expressed until division. Thus, the PIP-FUCCI reporter
478 system enables accurate delineation of G1/S and S/G2. M phase is marked by nuclear
479 envelope breakdown and diffusion of mVenus and mCherry signals throughout the cell.
480 Mitosis and cytokinesis can also be monitored by DNA stain and DIC imaging (Fig. 5C).
481 Following cytokinesis, only mVenus is expressed in the two daughter cell nuclei, marking
482 G1. A schematic of cell fluorescence expression and fluorescent intensity traces for
483 mVenus and mCherry throughout the cell cycle are shown in Fig. 5B.
484
485 To directly compare pHi and cell cycle, PIP-FUCCI was stably expressed in H1299 cells
486 (H1299-FUCCI) (Fig. 5C, Video S3), and we used pHi manipulation conditions to
487 experimentally lower and raise pHi. A combination of two small molecule inhibitors was
488 used to lower pHi: 5-(N-ethyl-N-isopropyl) amiloride (EIPA), which inhibits NHE1 (White
489 et al., 2017b) and 2-chloro-N-[[2′-[(cyanoamino)sulfonyl][1,1′-biphenyl]-4-yl]methyl]-N-[(4-
490 methylphenyl)methyl]-benzamide (S0859) (Larsen et al., 2012), which inhibits the $Na^+$-
491 $HCO_3^-$ transporter (NBCn1) (Fig. 5D). To raise pHi, low levels of ammonium chloride
492 ($NH_4Cl$) (White et al., 2017b) were used (Fig. 5D). We then used time-lapse confocal
493 microscopy to measure FUCCI reporter expression in cells over a 36 h period with and
494 without pHi manipulation. Single cells were tracked over time and mVenus and mCherry
495 fluorescent intensities were analyzed to determine lengths of single-cell cell cycle phases
496 (see methods for details). Cells that were in G1 phase at the start of treatment with E+S

497 (low pHi) and $NH_4Cl$ (high pHi) conditions were analyzed for successful completion of a
498 full cycle compared to untreated (control) cells (Fig. 5E). In both conditions, cells
499 successfully completed G1/S, but only 10.2% of low pHi cells successfully entered G2.
500 Subsequently, no low pHi cells starting in G1 phase could reach M phase and divide.
501 Cells in G1 with high pHi were able to complete the cell cycle at rates similar to control
502 cells (Fig 5E). Next, dividing cells in each treatment condition were plotted as single-cell
503 traces of FUCCI fluorescence intensities (mVenus, mCherry) and aligned to division time
504 (Fig. 5F-H). From these traces, we observed overall fewer divisions for low pHi cells
505 (37.5%), and only low pHi cells in G2 or M phase at the start of treatment were able to
506 divide (Fig. 5F). High pHi induced phase elongation in parental cells prior to division, read
507 out by elongated mVenus and mCherry traces compared to control (Fig. 5H). G1 phase
508 (high mVenus, low mCherry) is appreciably shortened in daughter cells at low pHi (Fig.
509 5F) while high pHi generally elongated G1 (Fig. 5H) compared to control (Fig. 5G).
510
511 To investigate this G1 phase shortening/elongation, we quantified all cell cycle phase
512 durations under control, high, and low pHi conditions. Using fluorescence intensity cutoffs
513 to determine G1/S and S/G2 (Fig. 5B, see methods), we measured significant differences
514 in phase durations with high and low pHi conditions (Fig. 5I-J, L). We found that G1 phase
515 in daughter cells was significantly shortened at low pHi (1.7±0.4 h) and significantly
516 elongated at high pHi (8.7±2.3h) compared to control cells (6.3±1.8 h) (Fig. 5I). These
517 pHi-dependent changes in G1 phase duration suggest that low pHi is a permissive cue
518 for G1 exit and that aberrant alkalization can delay this cell-cycle transition. These data
519 align with the measured decrease in pHi at G1/S in endpoint assays (Fig. 5A).

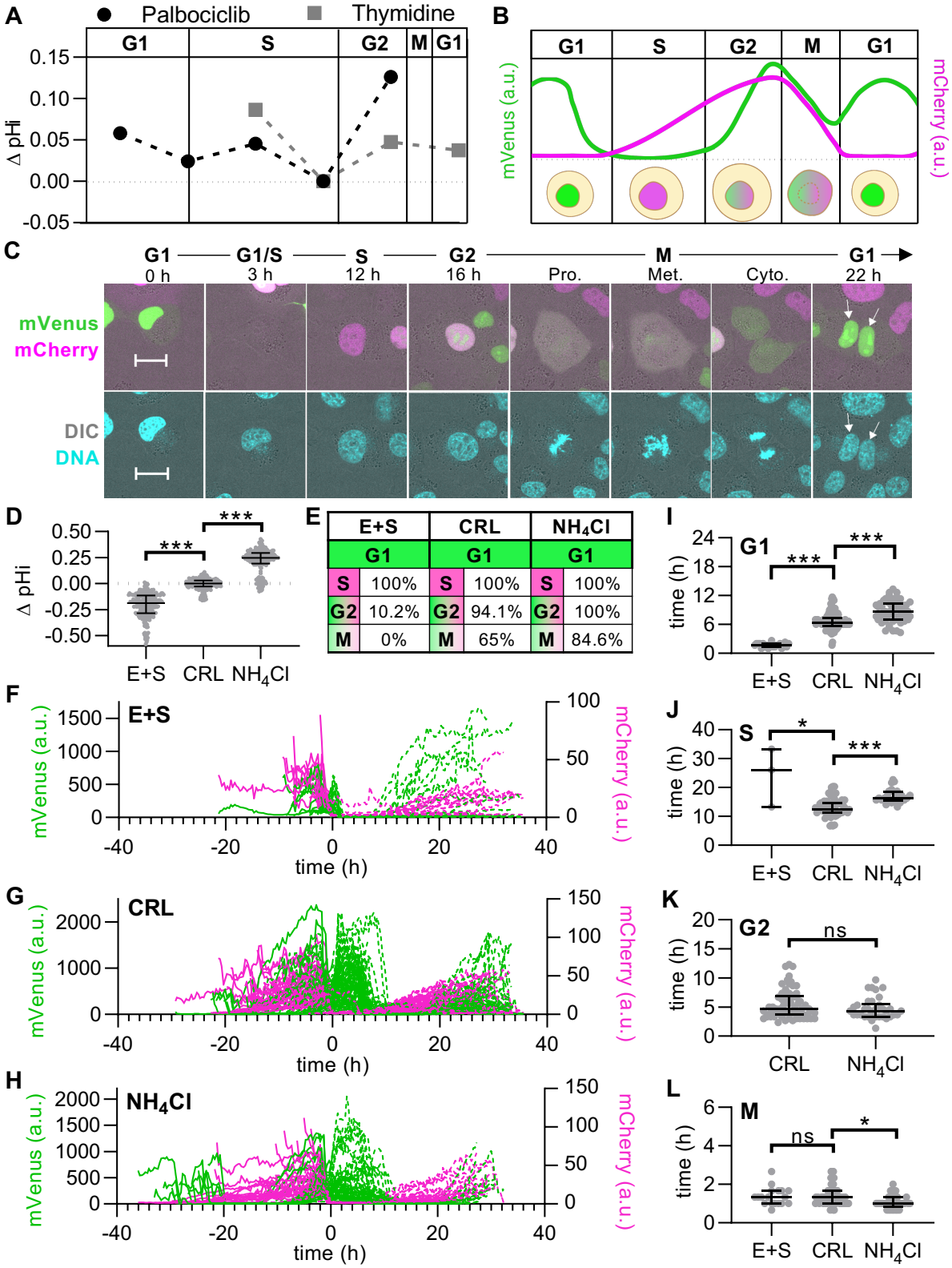


**Figure 5: pHi dynamics are key regulators of cell cycle and time G1 exit and S phase duration.** A) Median plots of single-cell delta pHi from peak cyclin B1 (thymidine, 4 h;

522 Palbociclib, 12 h). Data reproduced from Fig. 2I and 3I. (thymidine, n=4; Palbociclib, n=3)
523 B) Schematic of PIP-FUCCI reporter fluorescence traces and cell cycle phases (Grant et
524 al., 2018). C) Representative stills of Video S3. Shown is a single H1299-FUCCI cell with
525 PIP-mVenus (green) and mCherry-Geminin (magenta) tracked through each cell cycle
526 phase. Hoescht dye (DNA, cyan) and DIC merge shown and daughter cells indicated
527 (arrowheads); scale bars: 50 µm. D) Single-cell pHi of H1299-FUCCI cells treated with
528 EIPA and SO859 (E+S, n=233) to lower pHi, untreated (CRL, n=267), or treated with
529 ammonium chloride ($NH_4Cl$, n=202) to raise pHi (see methods for details). E) Progression
530 success of cells in G1 treated as in D. E+S (n=28), CRL (n=17), or $NH_4Cl$ (n=13). F-H)
531 PIP-mVenus (green) and mCherry-Geminin (magenta) fluorescence intensity traces from
532 single H1299-FUCCI cells treated as in D. Traces aligned at time of division at 0 h and
533 daughter cell pHi indicated by dotted lines: F) E+S, (n=23); G) CRL (n=126); H) $NH_4Cl$
534 (n=72). (CRL and $NH_4Cl$: 3 biological replicates, E+S, 2 biological replicates). I-L) Cell
535 cycle phase durations of cells in F-H. I) G1 (E+S, n=22; CRL, n=100; $NH_4Cl$, n=51) J) S
536 (E+S, n=3; CRL, n=67; $NH_4Cl$, n=26), K) G2 (CRL, n=65; $NH_4Cl$, n=34), and L) M (E+S,
537 n=18; CRL, n=77; $NH_4Cl$, n=33). For D and I-L, scatter plots (median±IQ range), with
538 Mann-Whitney test to determine statistical significance (*$p<0.05$; ***$p<0.001$).
539

540

541 After G1 phase completion, we found that high pHi significantly elongated S phase
542 (16.3±2.4 h) compared to control (12.3±3.0 h), while low pHi inhibited the S/G2 transition
543 for all but 10.4% of cells (Fig. 5J). This suggests that high pHi is a requirement for S phase
544 transition to G2, but there is also a need for low pHi for proper timing of S phase duration
545 compared to control cells. The requirement for an increase and decrease in pHi is
546 supported by our synchronized single-cell pHi data, which showed an increase in pHi
547 during mid-S phase and a decrease in late S phase or near the S/G2 transition (Fig. 5A).
548 Our data suggests that without an increase in pHi, cells cannot transition from S to G2
549 phase, but also that dynamic pHi is required for correct timing of S phase.

550

551 During G2 phase, we did not measure a significant difference in phase length with high
552 pHi compared to control (Fig. 5J). Low pHi cells could not complete the S/G2 transition,
553 therefore no G2 phase times could be measured. As previously mentioned, M phase

554 duration for low pHi cells could be measured only for cells in G2 or M during the start of
555 the experiment. We hypothesized that if a high pHi threshold was already met during early
556 G2, low pHi cells had the ability to complete division. This hypothesis aligns with our time-
557 lapse data showing high pHi 5 h prior to division followed by rapid acidification during
558 mitosis (Fig. 4C, S7C).
559 We were surprised to see a significant shortening of M phase with high pHi, as we
560 expected the lack of acidification to elongate M phase. However, previous work in lower-
561 order organisms showed that high pHi stabilizes microtubules (Gagliardi and Shain, 2013;
562 Schatten et al., 1986) and low pHi caused metaphase arrest (Watanabe et al., 1997), so
563 if cells can more rapidly assemble the spindle during early M phase, that could lead to a
564 shorter progression to division. While future work will explore the molecular mechanisms
565 driving the shortening/elongation of cell cycle phases, our results suggest that a decrease
566 in pHi is a cue for G1 exit, increases/decreases are required for S phase, and increases
567 are necessary for G2 entry.
568
569 These single-cell measurements, both via endpoint assays and single-cell time-lapse
570 measurements, show novel pHi dynamics through the cell cycle. Our data support prior
571 work using ion transporter knockdown to show that high pHi regulates S phase length
572 (Flinck et al., 2018b) and G2/M (Putney and Barber, 2003). However, our work also
573 reveals novel decreases in pHi during G1/S, late S, and mitosis (Fig. 6). Our combined
574 use of single-cell pHi manipulation and cell cycle reporters show that pHi plays an
575 important role in regulating the cell cycle, particularly for correct timing of G1 exit, S phase

progression, and G2 entry (Fig. 6. Our work suggests single-cell pHi not only reports on but regulates the essential cell function of cell cycle progression.

## DISCUSSION

Intracellular pHi dynamics have been implicated in diverse cellular processes like differentiation (Ulmschneider et al., 2016), proliferation (Flinck et al., 2018a), migration (Martin et al., 2011a), and apoptosis (Sergeeva et al., 2017). However, we have a limited mechanistic understanding of how spatiotemporal and single-cell pHi dynamics regulate cell behaviors. This is partially due to reliance on population analyses, non-physiological environments, or genetic ion transporter ablation approaches to link pHi and phenotype (Czowski et al., 2020).

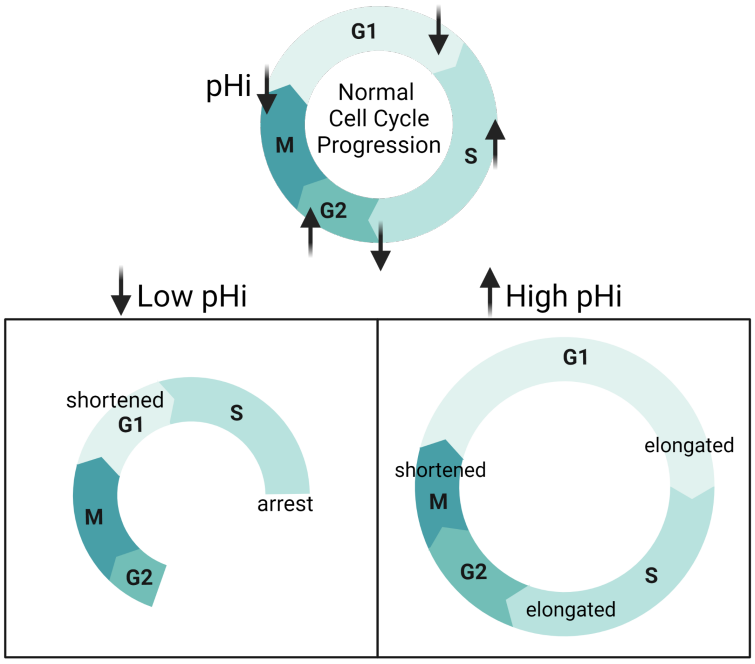


**Figure 6: Single-cell pHi is dynamic during cell cycle progression and regulates G1 exit, S phase duration, and S/G2 transition.** During cell cycle progression, pHi decreases at the G1/S boundary, increases in mid-S phase before dropping in late S, increases through G2 and decreases leading to division. When pHi is experimentally lowered, cells have a shortened G1 and S phase arrests. With high pHi conditions, G1 and S phases

592 are elongated, and M phase is shortened. This suggests that low pHi cues G1 exit and
593 high pH is necessary for G2 entry.
594

595 Here, we present two results linking single-cell pHi and non-genetic phenotype. First, our
596 single-cell pHi measurements confirm that pHi is heterogeneous even in genetically-
597 identical clonal cell lines, suggesting pHi may correlate with non-genetic phenotypic
598 variation. Second, we demonstrate using single-cell approaches that transformed cells
599 have a higher median pHi than normal cells, agreeing with population-level analyses that
600 suggest cancer cells have a constitutively increased pHi homeostasis compared to
601 normal cells (White et al., 2017a). However, our single-cell analyses reveal that pHi
602 heterogeneity is similar when compared across normal and transformed cell lines. This
603 result was surprising, as we hypothesized that pHi heterogeneity might reflect the
604 increased phenotypic heterogeneity in cancer (Hinohara and Polyak, 2019). A future goal
605 is to more closely examine whether pHi is predictive of phenotype (i.e. can pHi be used as a
606 biomarker of more cryptic phenotypic markers of cells such as cell cycle status, metabolic
607 activity, and growth factor signaling heterogeneity). The fact that in our data the average
608 pHi increased with metastatic potential suggests that pHi could be used to identify cancer
609 vs. normal tissue at the single-cell level.
610

611 We also characterized the relationship between pHi and cell cycle progression. Prior work
612 at the population level using genetic ablation of ion transporters and non-native
613 environments suggested a role for pHi in regulating cell cycle progression (Flinck et al.,
614 2018a). We show that single-cell pHi is dynamic over an entire cell cycle, with pHi
615 significantly decreasing at the G1/S boundary, increasing in mid-S before dropping in late
616 S phase, alkalinizing through G2 and peaking at G2/M, and finally acidifying during

617 mitosis followed by pHi recovery in daughter cells. Here, we present three key results
618 suggesting a regulatory link between pHi dynamics and cell cycle at both the population
619 and single-cell levels.
620
621 First, we show for that pHi significantly decreases at the G1/S boundary. These results
622 were consistent across multiple cell lines regardless of which cell cycle synchronization
623 method was used. Our single-cell pHi manipulation data suggest that decreased pHi is a
624 permissive cue for G1 exit. Low pHi significantly shortened G1, while high pHi conditions
625 significantly elongated G1 compared to control. These results indicate a novel regulatory
626 role for pHi acidification in regulating G1 exit.
627
628 Second, we show that pHi increases in mid-S phase and decreases before the S/G2
629 transition. Dynamic pHi, both increases and decreases, are important for proper timing of
630 S phase. Low pHi inhibited the S/G2 transition and while high pHi allowed for S/G2, these
631 cells spent a significantly longer time in S phase compared to control. The single-cell pHi
632 manipulation data suggests that increased pHi is necessary for successful entry into G2.
633 This confirms results at the population level showing pHi increases in S phase (Flinck et
634 al., 2018b) and successful transition through G2/M (Putney and Barber, 2003). But our
635 work also reveals novel decreases in pHi that may be necessary for successfully timed
636 G1/S and S/G2 transitions
637
638 Third, we show that single-cell pHi dynamics peak at G2/M and rapidly acidified during M
639 phase. The increase in pHi during G2/M confirms prior work showing that increased pHi

correlated with increased G2/M transition (Putney and Barber, 2003; Sellier et al., 2006). However, our data also suggest a novel role for intracellular acidification during late M phase and division. Future work using time-lapse imaging and applying optogenetic tools to spatiotemporally change pHi (Donahue et al., 2021) will be required to further characterize M phase pHi dynamics.

Single-cell techniques can elucidate single-cell behaviors and heterogeneity not found at the population level. Here, we addressed a critical need in the field to understand how pHi dynamics regulate single cells during cell cycle progression. These pHi dynamics could be essential for understanding complex cell biology that integrates single-cell and tissue-level behaviors. For example, prior work showed pHi gradients are generated in morphogenetic tissues (Weiß and Bohrmann, 2019). Our work now supports the hypothesis that bursts of synchronized cell proliferation may underlie these observations. More work is necessary to determine how temporal pHi gradients occur during cell cycle phase transitions and whether a threshold of pHi changes is required. With our data establishing a framework of pHi regulation during an entire cell cycle, future work will determine which pH-sensitive proteins may be mediating and correctly timing pH-dependent cell cycle progression. The knowledge gained could aid in identifying new therapeutic routes for limiting proliferation and pHi-dependent behaviors in cancer progression.

662 **MATERIALS AND METHODS**

663 **Cell Culture and Conditions**

664 Complete media for H1299 cells (ATCC CRL-5803): RPMI 1640 (Corning, 10-040-CV)
665 supplemented with 10% Fetal Bovine Serum (FBS, Peak Serum, PS-FB2); A549 (ATCC
666 CCL-185): DMEM (Corning, MT10013CVV) supplemented with 10% FBS; and NL20
667 (ATCC CRL-2503): Ham's F12 (Lonza, 12001-578) supplemented with 4% FBS, 1.5 g/L
668 sodium bicarbonate (Sigma, S6014), 2.7 g/L glucose (VWR, BDH9230), 2.0 mM
669 Glutamax (Gibco, 35050079), 0.1 mM nonessential amino acids (Lonza, BW13114E),
670 0.005 mg/mL insulin (Sigma, I1882), 10 ng/mL EGF (Peprotech, AF-100-15), 0.001
671 mg/mL transferrin (BioVision, 10835-642), 0.0005 mg/mL hydrocortisone (Sigma,
672 H0888). All cells were maintained at 5% $CO_2$ and 37°C in a humidified incubator.

673

674 **Transfections and stable cell line selection**

675 H1299 cells were transfected with the pCDNA3-mCherry-SEpHluorin (Koivusalo et al.,
676 2010) (mCh-pHl) or pLenti-CMV-Blast-PIP-FUCCI using Lipofectamine2000 (Life
677 Technologies, 11668019) per manufacturer's instructions. After 24 h, cells were
678 trypsinized and plated at low dilution in a 10 cm dish with media containing 0.8 mg/mL
679 Geneticin. Cloning cylinders were used to select colonies expressing mCh-pHl for
680 expansion. A final clone was selected based on microscopy assay for mCh-pHl
681 expression and comparison of cell morphology and pHi to parental H1299. For H1299-
682 FUCCI, cells were trypsinized after 24 h transfection and plated at low dilutions (50
683 cells/mL) in a 96 well plate in media containing 0.5 mg/mL Blasticidin. Wells with equal

684 expression were further expanded and screened on a microscopy assay for FUCCI
685 expression and for similar cell morphology and pHi compared to parental H1299.
686
687 Lentiviral transfection was used to generate stable mCh-pHl expression in NL20 and
688 A549 cells. Production of the virus was carried out in 293FT cells. Cells were grown to
689 near confluency in a 10 cm dish and transfected with plx304-mCherry-SEpHluorin (Gift of
690 Yi Liu and Diane Barber at UCSF) and two packaging plasmids: PSPAX2 (Addgene
691 #12260) and PMD2.6 (Addgene #12259) provided by Siyuan Zhang (University of Notre
692 Dame). Three µg each of the plx304-mCherry-pHluorin, PSPAX2, and PDM2.6 were
693 transfected into a nearly confluent 10 cm dish of 293FT cells using Lipofectamine2000
694 for 18 h. Media was changed and incubated another three days. Viral supernatant was
695 collected from the cells and centrifuged for 15 min at 3000 rpm. The supernatant was
696 passed through a 0.2 µm polyethersulfone filter, flash-frozen in liquid nitrogen in 1 mL
697 aliquots, and stored at -80°C.
698
699 NL20 and A549 cells were plated in a 6-well plate for viral transduction. After 24 h, viral
700 supernatant was diluted 1:1.6, 1:3, and 1:10 into antibiotic-free media (depending on cell
701 line) with 10 µg/mL Polybrene (Sigma, TR-1003-G), added to separate wells and
702 incubated for 48-72 hr. Transduced cells were moved to a 10 cm dish and selected with
703 0.5 mg/mL Blasticidin (Fisher, BP264725). NL20 cells were plated at low density in 96
704 well plates (0.5 cells/well). Colonies expressing mCh-pHl were expanded, and a final
705 NL20-mCh-pHl clone was chosen based on microscopy assay for mCh-pHl expression
706 and comparison to morphology and pHi of parentals. A549 cells were sorted using

707 fluorescence-activated cell sorting (FACS), and a population sort according to mCherry
708 expression was used for all imaging experiments after confirmation with microscopy.
709

710 **BCECF plate reader assays**

711 Cells were plated at $4.0x10^5$ - $8.0x10^5$ cells/well in a 24-well plate and incubated
712 overnight. Cells were treated with 2 μM 2',7'-Bis-(2-Carboxyethyl)-5-(and-6)-
713 Carboxyfluorescein, Acetoxymethyl Ester (BCECF-AM) (VWR, 89139-244) for 30 min at
714 37°C and 5% $CO_2$. NL20 and H1299 cells were washed 3x5 minutes with a pre-warmed
715 (37°C) HEPES-based wash buffer (30 mM HEPES pH 7.4, 145 mM NaCl, 5 mM KCl, 10
716 mM glucose, 1 mM $MgSO_4$, 1 mM $KHPO_4$, 2 mM $CaCl_2$, pH 7.4) and A549 cells were
717 washed 3x5 minutes with a pre-warmed (37°C) Bicarbonate ($HCO_3$)-based wash buffer
718 (25 mM $HCO_3$, 115 mM NaCl, 5 mM KCl, 10 mM glucose, 1 mM $MgSO_4$, 1 mM $KHPO_4$,
719 2 mM $CaCl_2$, pH 7.4). Two Nigericin buffers (25 mM HEPES, 105 mM KCl, 1 mM $MgCl_2$)
720 were supplemented with 10 μM nigericin (Fisher, N1495), pH was adjusted to ~6.7 and
721 ~7.7, and were pre-warmed to 37°C. Fluorescence was read (ex 440, em 535; ex 490,
722 em 535) on a Cytation 5 plate reader incubated at 37°C with 5% $CO_2$. Kinetic reads were
723 taken at 15-sec intervals for 5 min, using a protocol established within Gen5 software.
724 After the initial pHi read, the HEPES/bicarbonate wash was aspirated and replaced with
725 one of the nigericin buffer standards, and cells were incubated at 37°C with 5% $CO_2$ for 7
726 min. BCECF fluorescence was read by plate reader as above. This process was repeated
727 with the second nigericin standard. The mean intensity ratio (490/440) was derived from
728 each read. Measurements were calculated from a nigericin linear regression using exact
729 nigericin buffer pH to the hundredths place (Grillo-Hill et al., 2014).

730

731 **Microscopy**

732 Imaging protocol was derived from Grillo-Hill et al. Cells were plated on a 35 mm imaging
733 dish with a 14 mm glass coverslip (Matsunami, D35-14-1.5-U) a day before imaging.
734 Microscope objectives were preheated to 37°C, and the stage-top incubator was
735 preheated to 37°C and kept at 5% $CO_2$/95% air. Confocal images were collected on a
736 Nikon Ti-2 spinning disk confocal with a 40x (CFI PLAN FLUOR NA1.3) oil immersion
737 objective. The microscope is equipped with a stage-top incubator (Tokai Hit), a Yokogawa
738 spinning disk confocal head (CSU-X1), four laser lines (405nm, 488nm, 561 nm, 647 nm),
739 a Ti2-S-SE motorized stage, multi-point perfect focus system, and an Orca Flash 4.0
740 CMOS camera. Hoescht dye (405 laser ex, 455/50 em), pHluorin (488 laser ex, 525/36
741 em), TxRed (561 laser ex, 605/52 em), and mCherry (561 laser ex, 630/75 em) were
742 used. Acquisition times for each fluorescence acquisition ranged from 100-800
743 milliseconds.

744 For imaging, initial fields of view (FOV) were collected on the cells in their respective
745 media. For all imaging, nigericin buffers were prepared identically to BCECF assays, and
746 all buffer exchanges were carried out on the stage incubator to preserve XY positioning.
747 Multiple Z-planes were collected with the center focal plane maintained using a Perfect
748 Focus System (PFS).

749

750 **Single-cell pHi measurements**

751 After acquisition, NIS Analysis Software was used to quantify pHi. Images were
752 background-subtracted using an ROI drawn on a glass coverslip (determined by DIC).

753 Individual Regions of Interest (ROI) are drawn for each cell in each condition (initial, high
754 pH nigericin, and low pH nigericin), and mCherry aggregates are removed using
755 thresholding holes. Mean pHluorin and mCherry pixel intensities were quantified for each
756 cell, and pHluorin/mCherry ratios were calculated in excel. A cutoff of 100 a.u. units were
757 used for both pHluorin and mCherry intensity values after exporting. For each cell,
758 nigericin values were used to generate a standard curve, and pHi was back-calculated
759 from the single-cell standard curve.
760
761 **Double-Thymidine block**
762 Cells were plated at 10% confluency in 5 replicate 35 mm glass-bottomed dishes and 5
763 replicate 6-well plates (for protein lysate collection) and incubated overnight. Dishes were
764 identically treated with 2 mM thymidine (Sigma, T9250) for 18 h, washed with PBS, and
765 incubated with fresh complete media for 9 h, then treated for another 18 h with 2 mM
766 thymidine. Cells were released with a PBS wash and fresh complete media. Imaging of
767 the 0 h time point was initiated 20 min after release. Subsequent imaging was collected
768 at 4, 8, 12, and 24 h after release in respective media. Matched dishes at each time point
769 were washed twice with PBS and frozen at -80°C for protein lysate collection and
770 immunoblot analysis of cyclins.
771
772 For time-lapse imaging, the double-thymidine block was used as explained above on a
773 single 35 mm glass-bottomed dish supplemented with 1% Pen/Strep (Corning, 30-001-
774 C1) to avoid bacterial contamination during long-term acquisition. Hoechst 33342 solution
775 (ThermoFisher, 62249) was added to the cells (1:20,000) before release and incubated

776 for 15 min. Dye and thymidine were removed, and cells were washed with PBS to release
777 cells. Fresh media was added, and images were collected every 20 min for 24 hr. Optimal
778 acquisition parameters were as follows: 700 ms exposure time and 8% laser power for
779 GFP; 700 ms exposure time and 10% laser power for TxRed; and 100 ms exposure time
780 and 5% laser power DAPI. A single Z-plane was collected to avoid photobleaching.
781 Nigericin standards were carried out as previously described (Grillo-Hill et al., 2014).
782

783 **Palbociclib Synchronization**

784 Cells were plated at 10% confluency in 5 replicate 35 mm glass-bottomed dishes and 5
785 replicate 6-well plates (for protein lysate collection) and incubated overnight. Dishes were
786 identically treated with 0.1 μM Palbociclib (PD-0332991) (Selleck, S1116) for 24 h. Cells
787 were washed with PBS and released with complete fresh media. Imaging of the 0 h time
788 point was initiated 20 min after release. Subsequent imaging was collected at 4, 8, 12,
789 24, and 36 h post-release in respective media (1 replicate 0-24 h, 2 replicates 0-36 h).
790 Matched dishes at each time point were washed twice with PBS and frozen at -80°C for
791 protein lysate collection and immunoblot analysis of cyclins.
792

793 **FUCCI cell cycle assays**

794 For H1299-FUCCI time-lapses, cells were plated in a 4 well imaging dish (10,000
795 cells/well) and supplemented with 1% Pen/Strep (Corning, 30-001-C1) to avoid bacterial
796 contamination during long-term acquisition. Hoechst dye was added to the cells
797 (1:20,000) 6-8 h prior to imaging and incubated for 15 min, dye solution was removed,
798 and fresh media was added to the cells. Cells were imaged just prior to pHi manipulation,

799 then treatments were added to the cultured media and images were collected every 20
800 min for 36 hr. Optimal acquisition parameters were as follows: 200 ms exposure time
801 and 8% laser power for mVenus; 800 ms exposure time and 10% laser power for
802 mCherry; and 200 ms exposure time and 5% laser power DAPI. A single Z-plane was
803 collected to avoid excess light. Additional water was added to the stage top incubator at
804 18 h.
805
806 After acquisition, NIS Analysis Software was used to quantify individual cell cycle phases.
807 Images were background-subtracted using an ROI drawn on a glass coverslip
808 (determined by DIC). Cells were tracked using NIS Analysis software and nuclear regions
809 of interest (ROI) based on DNA stain. In case of improper tracking, manual tracking was
810 used to redraw ROIs. Manual tracking was also used during mitosis when the signals
811 diffused throughout the cell. mVenus and mCherry intensities were exported from
812 matched single-cell nuclear ROI at each time point over 36 h.
813
814 Cell cycle phases were determined by mVenus or mCherry fluorescence intensity. For
815 each individual cell trace, including subsequent daughter cells, an excel macro was used
816 to determine timepoints for mVenus and mCherry cutoffs. G1/S was defined as a
817 decrease in mVenus signal below 5% of maximum mVenus intensity. As validation of
818 G1/S, S phase entry was defined as the first time point after mCherry minimum that
819 showed a 3% (determined from mCherry maximum) increase in mCherry intensity
820 compared to the previous point. S/G2 was defined as point at which mVenus intensity

821 rose above 2% of mVenus maximum. G2/M and M/G1 were defined by nuclear envelope
822 breakdown and division into two daughter cells, respectively.
823
824 For pHi manipulation validation, cells were plated at 20% confluency on a 35 mm imaging
825 dish with a 14 mm glass coverslip and incubated overnight. Cells were treated with a
826 combination of 15 μM EIPA/30 μM SO859 (E+S) or 20 mM $NH_4Cl$ ($NH_4Cl$) diluted in fresh
827 media and incubated for 24 h. Both imaging collection and pHi calculations were
828 completed identically to other single-cell pHi measurement experiments. Treated cells
829 were corrected for photobleaching by collecting images of cells in nigericin buffers (pH
830 7.4) with treatment supplemented but without nigericin present.
831
832 **Western Blot**
833 Protein lysates were collected from 35-mm dishes or 6-well plates frozen at time points
834 matched to imaging. Ice-cold lysis buffer [50 mM TRIS, 150 mM NaCl, 1 mM dithiothreitol
835 (DTT), 1 mM Ethylenediaminetetraacetic acid (EDTA), 1% Triton X-100, Roche Protease
836 Inhibitor Cocktail] was added to the samples and incubated for 15 min on ice. Cells were
837 scraped and centrifuged for 10 min at 13,000 g at 4°C. The supernatant was retained,
838 and protein concentration was determined by Pierce™ BCA (ThermoFisher, 23225)
839 protein assay.
840
841 15 μg protein was loaded onto an SDS-Polyacrylamide gel electrophoresis (PAGE) that
842 was run for 3 h at 120 V in 1X Tris-glycine (3.02 g/L Tris, 14.4 g/L glycine, 1.0 g/L SDS).
843 Either a wet-transfer system or a Trans-Blot Turbo Transfer System (Bio-Rad) was used

844 to transfer the proteins to a polyvinylidene fluoride (PDVF) membrane (pre-wet with
845 methanol). For the wet transfer, 1X transfer buffer (141 g/L Glycine, 0.3 g/L Tris base)
846 with 20% Methanol for 1.5 h at 100 V. For the Trans-Blot Turbo Transfer, Bio-Rad transfer
847 buffer was used according to the manufacturer's protocol (7 min). Membranes were
848 blocked in 5% BSA in TBST (2.42 g/L Tris, 8 g/L NaCl, 0.1% Tween) for 2 h then divided
849 for blotting. Primary antibodies: α-cyclin A2 (1:500; Abcam, ab38), α-cyclin B1 (1:1,000;
850 Cell Signaling, 12231), α-cyclin E1 (1:1000; Cell Signaling, 4129), actin (1:1,000; Santa
851 Cruz, 2Q1055). Membranes were incubated with primary antibody solution overnight at
852 4°C with shaking (4 h at RT with shaking for actin). Membranes were washed 3x10 min
853 TBST at RT with shaking and incubated with secondary antibodies [1:10,000; goat α-
854 mouse IgG HRP (Bio-Rad, 1721011) or goat α-rabbit IgG HRP (Bio-Rad, 1706515)] for 2
855 h at RT with shaking. Membranes were washed 3x10 min TBST at RT with shaking,
856 developed using SuperSignal™ West Pico PLUS Chemiluminescent Substrate
857 (ThermoFisher, 34578), and visualized using a ChemiDoc MP Imaging System (BioRad).
858 ImageJ was used for protein quantification, normalized to loading control.
859

860 **Quantification and Statistics**

861 GraphPad Prism was used to prepare graphs and perform statistical analyses. Normality
862 tests were performed on all data sets and an outlier test using the ROUT method (Q=1%).
863 An unpaired t-test (Fig. S1, Fig. 4D) or paired t-test (Fig. 2F-H; Fig. 3F-H) was used for
864 normal data. A Mann Whitney test was used for non-normal, unpaired data (Fig. 1F-G,
865 Fig. S1, Fig. S3C, Fig. S4C, Fig. S6C, Fig, 5D, 5I-L). For time-lapse data (Fig. 4C, Fig.
866 4G, Fig. S7C), a one-sample Wilcoxon test was used, compared to a theoretical mean of

867 0. For non-normal, unpaired data with more than two sets, a Kruskal-Wallis test with
868 Dunn's multiple comparisons test was used (Fig. 2D and 2I, Fig. S3A, Fig. 3D, Fig. 3I,
869 Fig. S5C, Fig. S5E, Fig. S6A). Values were binned at 0.02 in all frequency distributions.
870 All significance was indicated in figures by the following: *$p<0.05$; **$p<0.01$; ***$p<0.001$.
871

872 **Online supplemental material**

873 Fig. S1 shows that the stable mCh-pHl biosensor expression does not alter pHi
874 compared to parental cell lines. Fig. S2 shows nigericin standardization and
875 pHluorin/mCherry ratios form a standard line to calculate pHi reliably. Fig. S3 shows
876 additional H1299-mCh-pHl Palbociclib synchronization replicates of Fig. 2. Fig. S4
877 shows additional H1299-mCh-pHl thymidine synchronization replicates of Fig. 3. Fig. S5
878 shows that pHi is dynamic after release from G1/S in A549-mCh-pHl cells and
879 correlates with cyclin levels. Fig S6 shows additional A549-mCh-pHl thymidine
880 synchronization replicates of Fig. S5. Fig. S7 illustrates heterogeneous timing of
881 prophase but preserved pHi changes from time-lapse experiments shown in Fig. 3. Fig.
882 S8 shows maturation rates of pHluorin and mCherry and no differences in fluorescent
883 protein synthesis between dividing and nondividing cells. Video 1 was used to produce
884 from Fig. 4A and 4B and demonstrates that the pHi of a dividing cell is dynamic
885 following release from G1/S. Video 2 was used to produce Fig. 4E and 4F and shows
886 that pHi dynamics of a nondividing cell are attenuated following release from G1/S.
887 Video 3 was used to produce Fig. 5C and shows an H1299-FUCCI cell differentially
888 expressing mVenus and mCherry depending on cell cycle phase.
889
890 **Video 1: Single, dividing cell shows dynamic pHi changes during cell cycle**
891 **progression.** Video of a dividing cell over 24 h (20 min intervals). Ratiometric display of
892 pHluorin/mCherry fluorescence ratios. Stills from this video were used to produce Fig. 4A, and
893 ratiometric scale is identical. Annotations show cell of interest and timing of
894 prophase/cytokinesis. Arrows reappear to show two daughter cells, scale bars: 20 μm.

895 **Video 2: Single, non-dividing cell shows attenuated pHi changes during over a 24-hour**
896 **period.** Video of a non-dividing cell over 24 h (20 min intervals). Ratiometric display of
897 pHluorin/mCherry fluorescence ratios. Stills from this video were used to produce Fig. 4E, and
898 ratiometric scale is identical. Annotations show cell of interest at the beginning and end of video,
899 scale bars: 20 μm.

900 **Video 3: PIP-FUCCI accurately reports cell cycle phases using mVenus and mCherry**
901 **expression in H1299 cells.** Video of a dividing H1299-FUCCI cell over 24 h (20 min intervals).
902 Fluorescent imaging of FUCCI reporters (PIP-mVenus, green) and (mCherry-Geminin$_{1-110}$,
903 magenta) that are differentially expressed through cell cycle. Labels appear as the cell transitions
904 to each phase (G1, S, G2, M, G1), scale bar: 20 μm. Stills from this video were used to produce
905 Fig. 5C.

906

## ACKNOWLEDGEMENTS

We would like to thank Dr. Siyuan Zhang (University of Notre Dame) and Dr. Diane Barber (University of California San Francisco) for plasmids. We would also like to thank members of the White lab for their helpful feedback on the manuscript. Figure schematics created with BioRender.com.

## COMPETING INTERESTS

The authors declare no competing financial or non-financial interests.

## FUNDING

This work was supported by a DP2 (1DP2CA260416-01) to K.A.W.

## AUTHOR CONTRIBUTIONS

JSS & KAW Conception and design. JSS acquisition of data. JSS & KAW analysis and interpretation of data, drafting and revising the article.

## REFERENCES

Aerts, R.J., A.J. Durston, and W.H. Moolenaar. 1985. Cytoplasmic pH and the regulation of the dictyostelium cell cycle. *Cell*. 43:653–657. doi:10.1016/0092-8674(85)90237-5.

Barth, D., and M. Fronius. 2019. Shear force modulates the activity of acid-sensing ion channels at low pH or in the presence of non-proton ligands. *Sci. Rep.* 9.

930 doi:10.1038/s41598-019-43097-7.
931 Bjursell, G., and P. Reichard. 1973. Effects of thymidine on deoxyribonucleoside
932 triphosphate pools and deoxyribonucleic acid synthesis in Chinese hamster ovary
933 cells. *J. Biol. Chem.* 248:3904–3909. doi:https://doi.org/10.1016/S0021-
934 9258(19)43819-2.
935 De Boer, L., V. Oakes, H. Beamish, N. Giles, F. Stevens, M. Somodevilla-Torres, C.
936 DeSouza, and B. Gabrielli. 2008. Cyclin A/cdk2 coordinates centrosomal and
937 nuclear mitotic events. *Oncogene*. 27:4261–4268. doi:10.1038/onc.2008.74.
938 Bolderson, E., J. Scorah, T. Helleday, C. Smythe, and M. Meuth. 2004. ATM is required
939 for the cellular response to thymidine induced replication fork stress. *Hum. Mol.*
940 *Genet.* 13:2937–2945. doi:10.1093/hmg/ddh316.
941 Boron, W.F. 2004. Regulation of intracellular pH. *Am. J. Physiol. - Adv. Physiol. Educ.*
942 28:160–179. doi:10.1152/advan.00045.2004.
943 Bryne Ulmschneider, Bree K. Grillo-Hill, Marimar Benitez, Dinara R. Azimova, D.L.B.
944 and T.G.N. 2016. Increased intracellular pH is necessary for adult epithelial and
945 embryonic stem cell differentiation. *J. Cell Biol.* 215:345–355.
946 doi:10.1083/jcb.201606042.
947 Cardone, R.A., V. Casavola, and S.J. Reshkin. 2005. The role of disturbed pH dynamics
948 and the NA+/H+ exchanger in metastasis. *Nat. Rev. Cancer*. 5:786–795.
949 doi:10.1038/nrc1713.
950 Chang, D.C., N. Xu, and K.Q. Luo. 2003. Degradation of cyclin B is required for the
951 onset of anaphase in mammalian cells. *J. Biol. Chem.* 278:37865–37873.
952 doi:10.1074/jbc.M306376200.

953 Chen, G., and X. Deng. 2018. Cell Synchronization by Double Thymidine Block. *Bio-*
954 *Protocol*. 8. doi:10.21769/bioprotoc.2994.
955 Choi, C.H., B.A. Webb, M.S. Chimenti, M.P. Jacobson, and D.L. Barber. 2013. pH
956 sensing by FAK-His58 regulates focal adhesion remodeling. *J. Cell Biol.* 202:849–
957 859. doi:10.1083/jcb.201302131.
958 Czowski, B.J., R. Romero-Moreno, K.J. Trull, and K.A. White. 2020. Cancer and pH
959 dynamics: Transcriptional regulation, proteostasis, and the need for new molecular
960 tools. *Cancers (Basel).* 12:1–19. doi:10.3390/cancers12102760.
961 Deutsch, C., J.S. Taylor, and D.F. Wilson. 1982. Regulation of intracellular pH by
962 human peripheral blood lymphocytes as measured by 19F NMR. *Proc. Natl. Acad.*
963 *Sci. U. S. A.* 79:7944–7948. doi:10.1073/pnas.79.24.7944.
964 Donahue, C.E.T., M.D. Siroky, and K.A. White. 2021. An Optogenetic Tool to Raise
965 Intracellular pH in Single Cells and Drive Localized Membrane Dynamics. *J. Am.*
966 *Chem. Soc.* 143:18877–18887. doi:10.1021/jacs.1c02156.
967 Flinck, M., S.H. Kramer, and S.F. Pedersen. 2018a. Roles of pH in control of cell
968 proliferation. *Acta Physiol.* 223:e13068. doi:10.1111/apha.13068.
969 Flinck, M., S.H. Kramer, J. Schnipper, A.P. Andersen, and S.F. Pedersen. 2018b. The
970 acid-base transport proteins NHE1 and NBCn1 regulate cell cycle progression in
971 human breast cancer cells. *Cell Cycle*. 17:1056–1067.
972 doi:10.1080/15384101.2018.1464850.
973 Fuster, D., O.W. Moe, and D.W. Hilgemann. 2004. Lipid- and mechanosensitivities of
974 sodium/hydrogen exchangers analyzed by electrical methods. *Proc. Natl. Acad.*
975 *Sci. U. S. A.* 101:10482–10487. doi:10.1073/pnas.0403930101.

976 Gagliardi, L.J., and D.H. Shain. 2013. Is intracellular pH a clock for mitosis? *Theor. Biol.*
977 *Med. Model.* 10. doi:10.1186/1742-4682-10-8.
978 Gillies, R.J., and D.W. Deamer. 1979. Intracellular pH changes during the cell cycle in
979 Tetrahymena. *J. Cell. Physiol.* 100:23–31. doi:10.1002/jcp.1041000103.
980 Grant, G.D., K.M. Kedziora, J.C. Limas, J. Gowen Cook, and J.E. Purvis. 2018.
981 Accurate delineation of cell cycle phase transitions in living cells with PIP-FUCCI.
982 doi:10.1080/15384101.2018.1547001.
983 Grillo-Hill, B.K., C. Choi, M. Jimenez-Vidal, and D.L. Barber. 2015. Increased H+ efflux
984 is sufficient to induce dysplasia and necessary for viability with oncogene
985 expression. *Elife*. 2015:1–31. doi:10.7554/eLife.03270.
986 Grillo-Hill, B.K., B.A. Webb, and D.L. Barber. 2014. Ratiometric Imaging of pH Probes.
987 *In* Methods in Cell Biology. 429–448.
988 Harguindey, S., D. Stanciu, J. Devesa, K. Alfarouk, R.A. Cardone, J.D. Polo Orozco, P.
989 Devesa, C. Rauch, G. Orive, E. Anitua, S. Roger, and S.J. Reshkin. 2017. Cellular
990 acidification as a new approach to cancer treatment and to the understanding and
991 therapeutics of neurodegenerative diseases. *Semin. Cancer Biol.* 43:157–179.
992 doi:10.1016/J.SEMCANCER.2017.02.003.
993 Hinohara, K., and K. Polyak. 2019. Intratumoral heterogeneity: more than just
994 mutations. *Trends Cell Biol.* 29:569–579. doi:10.1016/j.tcb.2019.03.003.
995 Karagiannis, J., and P.G. Young. 2001. Intracellular pH homeostasis during cell-cycle
996 progression and growth state transition in Schizosaccharomyces pombe. *J. Cell*
997 *Sci.* 2929–2941. doi:https://doi.org/10.1242/jcs.114.16.2929.
998 Korenchan, D.E., and R.R. Flavell. 2019. Spatiotemporal pH heterogeneity as a

999 promoter of cancer progression and therapeutic resistance. *Cancers (Basel).*
1000 11:1026. doi:10.3390/cancers11071026.
1001 Larsen, A.M., N. Krogsgaard-Larsen, G. Lauritzen, C.W. Olesen, S. Honoréhansen, E.
1002 Boedtkjer, S.F. Pedersen, and L. Bunch. 2012. Gram-Scale Solution-Phase
1003 Synthesis of Selective Sodium Bicarbonate Co-transport Inhibitor S0859: in vitro
1004 Efficacy Studies in Breast Cancer Cells. *ChemMedChem*. 7:1808–1814.
1005 doi:10.1002/CMDC.201200335.
1006 Lee, A.H., and I.F. Tannock. 1998. Heterogeneity of intracellular pH and of mechanisms
1007 that regulate intracellular pH in populations of cultured cells. *Cancer Res.* 58:1901–
1008 1908.
1009 Liu, M., H. Liu, and J. Chen. 2018. Mechanisms of the CDK4/6 inhibitor palbociclib (PD
1010 0332991) and its future application in cancer treatment (Review). *Oncol. Rep.*
1011 39:901–911. doi:10.3892/or.2018.6221.
1012 Lobo, R.C., N.E. Hubbard, P. Damonte, H. Mori, Z. Pénzváltó, C. Pham, A.L. Koehne,
1013 A.C. Go, S.E. Anderson, P.M. Cala, and A.D. Borowsky. 2016. Glucose Uptake and
1014 Intracellular pH in a Mouse Model of Ductal Carcinoma In situ (DCIS) Suggests
1015 Metabolic Heterogeneity. *Front. Cell Dev. Biol.* 4:93. doi:10.3389/fcell.2016.00093.
1016 Majdi, A., J. Mahmoudi, S. Sadigh-Eteghad, S.E.J. Golzari, B. Sabermarouf, and S.
1017 Reyhani-Rad. 2016. Permissive role of cytosolic pH acidification in
1018 neurodegeneration: A closer look at its causes and consequences. *J. Neurosci.*
1019 *Res.* 94:879–887. doi:10.1002/JNR.23757.
1020 Martin, C., S.F. Pedersen, A. Schwab, and C. Stock. 2011a. Intracellular pH gradients in
1021 migrating cells. *Am. J. Physiol. - Cell Physiol.* 300:490–495.

1022 doi:10.1152/AJPCELL.00280.2010.
1023 Martin, C., S.F. Pedersen, A. Schwab, and C. Stock. 2011b. Intracellular pH gradients in
1024 migrating cells. *https://doi.org/10.1152/ajpcell.00280.2010*. 300:490–495.
1025 doi:10.1152/AJPCELL.00280.2010.
1026 Mirkka Koivusalo, Christopher Welch, Hisayoshi Hayashi, Cameron C. Scott, Moshe
1027 Kim, Todd Alexander, Nicolas Touret, Klaus M. Hahn, and S.G. 2010. Amiloride
1028 inhibits macropinocytosis by lowering submembranous pH and preventing Rac1
1029 and Cdc42 signaling. *J. Cell Biol.* doi:10.1083/jcb.200908086.
1030 Putney, L.K., and D.L. Barber. 2003. Na-H Exchange-dependent Increase in
1031 Intracellular pH Times G2/M Entry and Transition. *J. Biol. Chem.* 278:44645–
1032 44649. doi:10.1074/jbc.M308099200.
1033 Rajal, A.G., K.A. Marzec, R.A. McCloy, M. Nobis, V. Chin, J.F. Hastings, K. Lai, M.
1034 Kennerson, W.E. Hughes, V. Vaghjiani, P. Timpson, J.E. Cain, D.N. Watkins, D.R.
1035 Croucher, and A. Burgess. 2021. A non-genetic, cell cycle-dependent mechanism
1036 of platinum resistance in lung adenocarcinoma. *Elife*. 10. doi:10.7554/ELIFE.65234.
1037 Reshkin, S.J., A. Bellizzi, S. Caldeira, V. Albarani, I. Malanchi, M. Poignee, M. Alunni-
1038 Fabbroni, V. Casavola, and M. Tommasino. 2000. Na + /H + exchanger-dependent
1039 intracellular alkalinization is an early event in malignant transformation and plays an
1040 essential role in the development of subsequent transformation-associated
1041 phenotypes. *FASEB J.* 14:2185–2197. doi:10.1096/fj.00-0029com.
1042 Schatten, G., T. Bestor, R. Balczon, J. Henson, and H. Schatten. 1986. Intracellular pH
1043 Shift Initiates Microtubule-Mediated Motility during Sea Urchin Fertilization. *Ann. N.*
1044 *Y. Acad. Sci.* 466:940–944. doi:10.1111/J.1749-6632.1986.TB38480.X.

1045 Sellier, C., J.F. Bodart, S. Flament, F. Baert, J. Cannon, and J.P. Vilain. 2006.
1046 Intracellular acidification delays hormonal G2/M transition and inhibits G2/M
1047 transition triggered by thiophosphorylated MAPK in xenopus oocytes. *J. Cell.*
1048 *Biochem.* 98:287–300. doi:10.1002/jcb.20764.
1049 Sergeeva, T.F., M. V. Shirmanova, O.A. Zlobovskaya, A.I. Gavrina, V. V. Dudenkova,
1050 M.M. Lukina, K.A. Lukyanov, and E. V. Zagaynova. 2017. Relationship between
1051 intracellular pH, metabolic co-factors and caspase-3 activation in cancer cells
1052 during apoptosis. *Biochim. Biophys. Acta - Mol. Cell Res.* 1864:604–611.
1053 doi:10.1016/j.bbamcr.2016.12.022.
1054 Siu, K.T., M.R. Rosner, and A.C. Minella. 2012. An integrated view of cyclin E function
1055 and regulation. *Cell Cycle*. 11:57–64. doi:10.4161/cc.11.1.18775.
1056 Taylor, I.W., and P.J. Hodson. 1984. Cell cycle regulation by environmental pH. *J. Cell.*
1057 *Physiol.* 121:517–525. doi:10.1002/jcp.1041210310.
1058 Trotter, E.W., and I.M. Hagan. 2020. Release from cell cycle arrest with Cdk4/6
1059 inhibitors generates highly synchronized cell cycle progression in human cell
1060 culture. *Open Biol.* 10:200200. doi:10.1098/RSOB.200200.
1061 Watanabe, K., M.S. Hamaguchi, and Y. Hamaguchi. 1997. Effects of Intracellular pH on
1062 the Mitotic Apparatus and Mitotic Stage in the Sand Dollar Egg. *Cytoskeleton*.
1063 37:263–270. doi:10.1002/(SICI)1097-0169(1997)37:3.
1064 Weiß, I., and J. Bohrmann. 2019. Electrochemical gradients are involved in regulating
1065 cytoskeletal patterns during epithelial morphogenesis in the Drosophila ovary. *BMC*
1066 *Dev. Biol.* 19. doi:10.1186/s12861-019-0203-y.
1067 White, K.A., B.K. Grillo-Hill, and D.L. Barber. 2017a. Cancer cell behaviors mediated by

1068 dysregulated pH dynamics at a glance. *J. Cell Sci.* 130:663–669.
1069 doi:10.1242/jcs.195297.
1070 White, K.A., D.G. Ruiz, Z.A. Szpiech, N.B. Strauli, R.D. Hernandez, M.P. Jacobson, and
1071 D.L. Barber. 2017b. Cancer-associated arginine-to-histidine mutations confer a
1072 gain in pH sensing to mutant proteins. *Sci. Signal.* 10.
1073 doi:10.1126/scisignal.aam9931.
1074